Circulation

ORIGINAL RESEARCH ARTICLE

MDM2 Regulation of HIF Signaling Causes Microvascular Dysfunction in Hypertrophic Cardiomyopathy

Puneeth Shridhar, MD, PhD; Michael S. Glennon, BS; Soumojit Pal, PhD; Christina J. Waldron, BS; Ethan J. Chetkof; Payel Basak, MD; Nicolas G. Clavere, PhD; Dipanjan Banerjee, PhD; Sebastien Gingras, PhD; Jason R. Becker, MD

BACKGROUND: Microvasculature dysfunction is a common finding in pathologic remodeling of the heart and is thought to play an important role in the pathogenesis of hypertrophic cardiomyopathy (HCM), a disease caused by sarcomere gene mutations. We hypothesized that microvascular dysfunction in HCM was secondary to abnormal microvascular growth and could occur independent of ventricular hypertrophy.

METHODS: We used multimodality imaging methods to track the temporality of microvascular dysfunction in HCM mouse models harboring mutations in the sarcomere genes *Mybpc3* (cardiac myosin binding protein C3) or *Myh6* (myosin heavy chain 6). We performed complementary molecular methods to assess protein quantity, interactions, and post-translational modifications to identify mechanisms regulating this response. We manipulated select molecular pathways in vivo using both genetic and pharmacological methods to validate these mechanisms.

RESULTS: We found that microvascular dysfunction in our HCM models occurred secondary to reduced myocardial capillary growth during the early postnatal time period and could occur before the onset of myocardial hypertrophy. We discovered that the E3 ubiquitin protein ligase MDM2 (murine double minute 2) dynamically regulates the protein stability of both HIF1α (hypoxia-inducible factor 1 alpha) and HIF2α (hypoxia-inducible factor 2 alpha)/EPAS1 (endothelial PAS domain protein 1) through canonical and noncanonical mechanisms. The resulting HIF imbalance leads to reduced proangiogenic gene expression during a key period of myocardial capillary growth. Reducing MDM2 protein levels by genetic or pharmacological methods normalized HIF protein levels and prevented the development of microvascular dysfunction in both HCM models.

CONCLUSIONS: Our results show that sarcomere mutations induce cardiomyocyte MDM2 signaling during the earliest stages of disease, and this leads to long-term changes in the myocardial microenvironment.

Key Words: capillaries ■ cardiomyopathy, hypertrophic ■ hypoxia ■ myocardium ■ myosin heavy chains ■ proteasome endopeptidase complex ■ sarcomere

Hypertrophic cardiomyopathy (HCM) is a disease characterized by pathologic thickening of the left ventricular (LV) myocardium which can lead to heart failure and sudden death in humans.[1] The prevalence of HCM in humans is ≈1:500 and mutations in sarcomere protein genes have been shown to cause this disease.[2] The most commonly mutated genes in HCM are *MYBPC3* (myosin binding protein C3) and *MYH7* (myosin heavy chain 7) and mutations in these 2 genes account for ≈80% of mutation-positive HCM cases.[3,4] The cause of myocardial hypertrophy in HCM is increased cardiomyocyte growth that occurs during childhood or in adult life in humans. However, pathologic ventricular remodeling in HCM is also associated with

Correspondence to: Jason R. Becker, MD, 200 Lothrop St, BST E1258, Pittsburgh, PA 15213. Email beckerj@pitt.edu
Supplemental Material is available at https://www.ahajournals.org/doi/suppl/10.1161/CIRCULATIONAHA.123.064332.
For Sources of Funding and Disclosures, see page 1885.
© 2023 The Authors. *Circulation* is published on behalf of the American Heart Association, Inc., by Wolters Kluwer Health, Inc. This is an open access article under the terms of the Creative Commons Attribution Non-Commercial-NoDerivs License, which permits use, distribution, and reproduction in any medium, provided that the original work is properly cited, the use is noncommercial, and no modifications or adaptations are made.
Circulation is available at www.ahajournals.org/journal/circ

Clinical Perspective

What Is New?

- We used 2 distinct murine models of hypertrophic cardiomyopathy and discovered that microvascular dysfunction in these models is secondary to reduced myocardial capillary formation.
- We discovered that the protein MDM2 (murine double minute 2) regulated this process through modulation of cardiomyocyte hypoxia-inducible factor signaling.
- Targeting MDM2 either genetically or pharmacologically increased myocardial capillary formation in both hypertrophic cardiomyopathy models and prevented microvascular dysfunction.

What Are the Clinical Implications?

- Microvascular dysfunction can develop early in the pathogenesis of hypertrophic cardiomyopathy and results from abnormalities in myocardial capillary formation, not regression.
- Targeting the MDM2 signaling pathway during the earliest stages of hypertrophic cardiomyopathy may be able to reduce the long-term sequela of microvascular dysfunction such as chronic angina and adverse ventricular remodeling.
- Sarcomere mutations can impact different stages of myocardial development and therapeutic strategies designed to exploit these developmental responses may successfully modify disease progression.

Nonstandard Abbreviations and Acronyms

CD31	cluster of differentiation 31
EPAS1	endothelial PAS domain-containing protein 1
HCM	hypertrophic cardiomyopathy
HIF1α	hypoxia-inducible factor 1 alpha
HIF2α	hypoxia-inducible factor 2 alpha
LCA	left coronary artery
LV	left ventricular
LVH	left ventricular hypertrophy
MDM2	murine double minute 2
MVD	microvascular dysfunction
MYBPC3	myosin binding protein C3
MYH6	myosin heavy chain 6
TIE2/TEK	tyrosine kinase with immunoglobulin-like loops and epidermal growth factor homology domains-2
VHL	Von Hippel-Lindau

changes in the noncardiomyocyte myocardial cell populations.[5] It remains incompletely understood how sarcomere protein mutations that are expressed primarily in the cardiomyocyte cell population lead to changes in the other cell types of the myocardium.

Microvascular dysfunction or disease (MVD), occurs secondary to abnormalities of the capillary beds of multiple different organs such as the brain, kidney, retina, skin, lung, and heart.[6–8] MVD has been consistently identified in many different forms of human cardiomyopathy secondary to both ischemic and nonischemic etiologies.[9–14] Mechanistically, MVD often involves an imbalance of proangiogenic and antiangiogenic factors which are critical for capillary formation and maintenance.[15] For example, reduced expression of the proangiogenic factors such as VegfA (vascular endothelial growth factor A) and angiopoietin 1 and 2 and increased production of the antiangiogenic factors angiopoietin 4 and thrombospondin 1, induce capillary rarefaction secondary to pressure overload.[16–19] However, the molecular mechanisms regulating the development of MVD in HCM remain poorly defined.

The prehypertrophic disease interval is a critical period in the development of HCM.[20–24] We hypothesized that MVD develops during this period secondary to alterations in cardiomyocyte signaling that can develop before the onset of hypertrophy. To explore these questions, we used multiple sarcomere gene mutant animal models of HCM to assess microvascular growth and dysfunction while exploring the key molecular mechanisms regulating these phenotypes. We then investigated if targeting these pathways was sufficient to prevent the development of MVD in preclinical models of HCM.

METHODS

All data needed to evaluate the conclusions in the article are present in the article or the Supplemental Material. Additional data related to this article may be requested from the authors. Detailed descriptions of materials and methods can also be found in the Supplemental Material.

Ethical Considerations

All mice used in the study were housed at American Association for the Accreditation of Laboratory Animal Care–accredited animal facility. The animal experiments were conducted in accordance with the practices defined in the Guide for the Care and Use of Laboratory Animals which were approved and overseen by the University of Pittsburgh institutional animal care and use committee.

Statistical Analysis

Experimental data was obtained in a blinded fashion to genotype or treatment group. Estimated sample sizes were calculated using preliminary experimental results. Statistical significance between 2 groups was calculated using 2-tailed unpaired Student *t* test. When unequal variances were detected using an F test, then the Welch *t* test was used. In the case of >2 groups, a 1- or 2-way ANOVA with a Tukey multiple comparisons test was used for determining statistical significance. When unequal variances were detected using a Brown–Forsythe test, then a

Brown–Forsythe and Welch ANOVA with Dunnett T3 multiple comparisons test was used for 1-way ANOVA. All statistical analyses were performed by Prism software version 9 (GraphPad). A P value <0.05 was considered statistically significant.

RESULTS

Reduced Postnatal Capillary Formation in Mybpc3$^{-/-}$ Myocardium Is Associated With MVD and Tissue Hypoxia

We previously found that deletion of the sarcomere protein MYBPC3 leads to early postnatal LV hypertrophy (LVH).[20] Therefore, we wanted to determine whether there was evidence of MVD in this model. First, we measured capillary-to-cardiomyocyte ratios in wild-type (WT) and Mybpc3$^{-/-}$ LV tissue by staining for the endothelial cell marker CD31 (cluster of differentiation 31). We discovered that capillary density was reduced in Mybpc3$^{-/-}$ LV tissue beginning at postnatal day 7 (Figure 1A and 1B; Figure S1A and S1B). Both male and female Mybpc3$^{-/-}$ mice had similar reductions in LV capillary density (Figure S1C). We then performed immunohistochemistry for an alternative endothelial cell marker, angiopoietin-1 receptor TIE2 (aka, TEK [tyrosine kinase]), and again found that capillary density was reduced at postnatal day 7 (Figure 1A and 1B; Figure S1D). We confirmed that CD31 and TIE2 detect the same cell population in the myocardium (Figure S1E and S1F). In addition to endothelial cells, pericytes are a critical cell population for proper capillary development.[25] Therefore, we performed immunohistochemistry for the pericyte marker NG2 (neural/glial antigen 2) and found that Mybpc3$^{-/-}$ mice also had reduced LV pericytes (Figure 1C and 1D; Figure S2A).

To complement the immunohistochemistry-based methods, we then injected fluorescently labeled tomato lectin which binds to vascular endothelial cells.[26] This allowed better visualization of the capillary lumens and confirmed that Mybpc3$^{-/-}$ mice had a significant reduction in LV capillaries (Figure 1E and 1F; Figure S2B and S2C, Videos S1 and S2). We confirmed that tomato lectin, CD31, and NG2 could detect the same myocardial capillaries (Figure S2D and S2E). In addition to reduced LV capillaries, we discovered that postnatal day 7 Mybpc3$^{-/-}$ mice had increased left coronary artery (LCA) dilation compared with WT control mice. However, LCA size was similar in both groups of mice after birth at postnatal day 2 arguing against a difference in embryonic coronary development between the groups (Figure S2F through S2I). Overall, these results show that LV capillary formation is reduced in the early postnatal period in Mybpc3$^{-/-}$ mice.

Next, we wanted to determine whether the reduction of LV capillaries in Mybpc3$^{-/-}$ mice led to microvasculature dysfunction. We measured blood flow in the LCA before and after the administration of the vasodilator adenosine to calculate the coronary flow reserve which is dependent on myocardial capillary blood flow (Figure 1G; Figure S2J through S2L).[27] Baseline myocardial blood flow was increased in Mybpc3$^{-/-}$ animals which was partly driven by the increased LCA size in these mice (Figure 1G and 1H). However, myocardial blood flow minimally increased after adenosine administration (Figure 1H). Therefore, the coronary flow reserve was reduced in Mybpc3$^{-/-}$ animals (Figure 1I). Next, we wanted to determine whether the MVD in Mybpc3$^{-/-}$ myocardium was associated with tissue hypoxia. We used the tissue hypoxia marker pimonidazole and detected a large increase in LV tissue hypoxia in Mybpc3$^{-/-}$ heart tissue (Figure 1J and 1K). Overall, these results show that the reduction of myocardial capillary formation in Mybpc3$^{-/-}$ mice leads to MVD and LV tissue hypoxia.

Dynamic Changes in HIF1α and HIF2α Occur During Early Postnatal Period in the Mybpc3$^{-/-}$ Myocardium

Since we detected tissue hypoxia in the Mybpc3$^{-/-}$ myocardium, we measured the protein levels of the hypoxia-regulated transcriptions factors HIF1α (hypoxia-inducible factor 1 alpha) and HIF2α (hypoxia-inducible factor 2 alpha)/EPAS1 (endothelial PAS domain protein 1).[28] We detected no differences in the protein levels at postnatal day 2 (Figure 2A and 2B). In contrast, there was a reduction of HIF1α protein and an increase of HIF2α in the Mybpc3$^{-/-}$ LV tissue at postnatal day 7 (Figure 2A and 2B). However, by postnatal day 25, the HIF1α and HIF2α LV protein levels were similar between WT and Mybpc3$^{-/-}$ mice (Figure 2A and 2B). We compared protein levels across the different ages and discovered that myocardial HIF1α protein levels do not increase at postnatal day 7 in the Mybpc3$^{-/-}$ LV tissue when compared with WT LV tissue (Figure 2C). In contrast, HIF2α protein levels increase at postnatal day 7 in Mybpc3$^{-/-}$ LV tissue and then return to control levels by postnatal day 25 (Figure 2D). We then performed immunohistochemistry to confirm that the changes in HIF1α and HIF2α protein levels were cardiomyocyte-specific (Figure 2E through 2G). Overall, these results show that during the early postnatal time period when myocardial capillary formation is reduced in the Mybpc3$^{-/-}$ mice, there are dynamic changes in cardiomyocyte HIF1α and HIF2α protein levels.

Noncanonical Degradation of HIF1α in the Mybpc3$^{-/-}$ Myocardium Is Regulated by Cardiomyocyte MDM2

We identified a reduction in HIF1α protein in the Mybpc3$^{-/-}$ myocardium at postnatal day 7. However, it was unclear whether the reduction of HIF1α protein was secondary to a reduction in gene expression or increased protein degradation. We found that despite the reduction

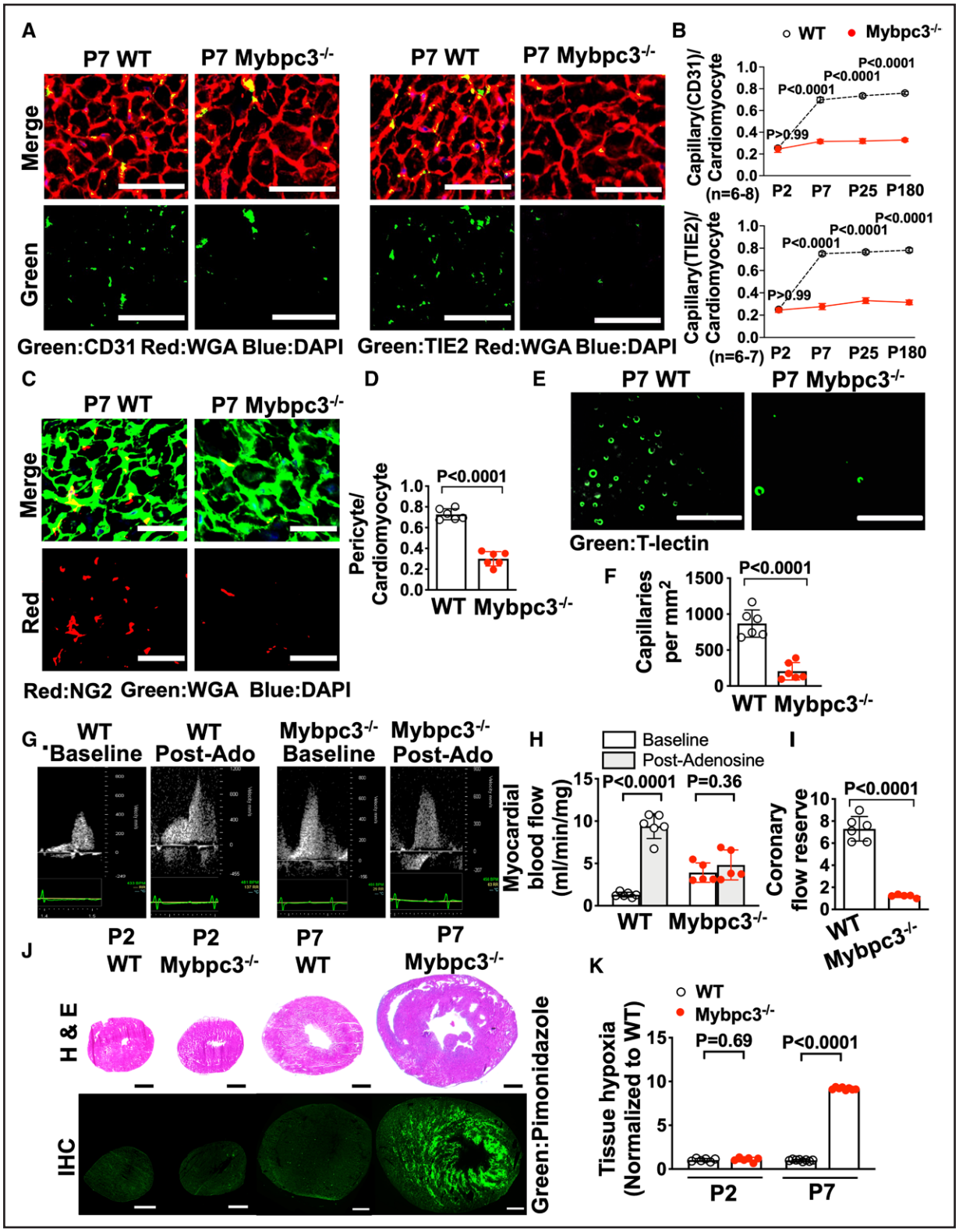

Figure 1. Reduced postnatal capillary formation in the Mybpc3$^{-/-}$ myocardium is associated with microvascular dysfunction and tissue hypoxia.

A, Representative immunohistochemistry images for the endothelial cell markers CD31 (**left**; green) or TIE2 (**right**; green) costained with WGA (red) in left ventricular tissue cross-sections from postnatal day 7 (P7) WT and Mybpc3$^{-/-}$ mice. Nuclei are blue (DAPI); scale bars=25 µm. **B**, Capillary-to-cardiomyocyte ratios from WT and Mybpc3$^{-/-}$ (n=6–8/group) left ventricular tissue at postnatal day 2 (P2), P7, postnatal day 25 (P25), or postnatal day 180 (P180). Capillaries were identified with CD31 (**top**) or TIE2 (**bottom**). Minimum 120 cardiomyocytes per sample. **C**, Representative immunohistochemistry images for the pericyte marker NG2 ([neural/glial antigen 2] red) costained with WGA (*Continued*)

Figure 1 Continued. (green) in left ventricular tissue from P7 WT and Mybpc3$^{-/-}$ mice. Nuclei are blue (DAPI); scale bars=25 µm. **D**, Pericyte-to-cardiomyocyte ratios from WT (n=6) and Mybpc3$^{-/-}$ (n=6) left ventricular tissue at P7. Minimum 200 cardiomyocytes per sample. **E**, Representative fluorescence images for the intravascularly injected endothelial cell stain, tomato lectin ([T-lectin] green) in left ventricular tissue from P7 WT and Mybpc3$^{-/-}$ mice. Scale bars=80 µm. **F**, Capillaries per mm^2 in WT (n=6) and Mybpc3$^{-/-}$ (n=6) left ventricular tissue at P7. Three cross-sectional images per sample were analyzed. **G**, Representative myocardial blood flow velocity tracings using pulsed wave Doppler echocardiography in postnatal day 60 WT and Mybpc3$^{-/-}$ mice. Myocardial blood flow at baseline and after retro-orbital injection with adenosine (postadenosine) to induce maximal hyperemia. **H**, Myocardial blood flow in postnatal day 60 WT after adenosine (light grey bars) were normalized to heart weight. **I**, Coronary flow reserve in postnatal day 60 WT (n=6) and Mybpc3$^{-/-}$ (n=5) mice. Coronary flow reserve is the ratio of myocardial blood flow after adenosine to myocardial blood flow at baseline. **J**, Representative H&E–stained heart cross-sections from P2 or P7 WT and Mybpc3$^{-/-}$ mice (**top**) and representative immunohistochemistry images of heart cross-sections from P2 or P7 WT and Mybpc3$^{-/-}$ mice injected with pimonidazole ([Hypoxyprobe] green; **bottom**). Scale bars=0.5 mm. **K**, Comparison of left ventricular tissue hypoxia in WT and Mybpc3$^{-/-}$ mice at P2 or P7 (n=6–8/group). Green fluorescent intensity for each sample was obtained and then normalized to P2 WT samples. All results are shown as mean±SEM. Student or Welch *t* tests were used for **D**, **F**, **H**, **I**, and **K**; 2-way ANOVA with Tukey multiple comparison test used for **B**. CD31 indicates cluster of differentiation 31; DAPI, 4′,6-diamidino-2-phenylindole; H&E, hematoxylin–eosin; IHC, immunohistochemistry; Mybpc3$^{-/-}$, cardiac myosin binding protein 3 homozygous deletion; Post-Ado, post adenosine; TIE2, TEK receptor kinase; WGA, wheat germ agglutinin; and WT, wild-type.

of HIF1α protein at postnatal day 7, there was increased Hif1α mRNA in Mybpc3$^{-/-}$ LV tissue (Figure 3A). Therefore, we hypothesized that there was increased degradation of HIF1α in the Mybpc3$^{-/-}$ myocardium. We administered the proteasomal inhibitor bortezomib and this normalized HIF1α protein (Figure 3B and 3C). We then performed an in situ proximity ligation assay to measure the amount of ubiquitinated HIF1α in the groups of mice that had been administered bortezomib. We discovered a robust increase in ubiquitinated HIF1α in the Mybpc3$^{-/-}$ LV tissue (Figure 3D and 3E; Figure S3A). These data show that the reduction of HIF1α in Mybpc3$^{-/-}$ LV tissue is secondary to increased ubiquitination and proteasomal degradation of HIF1α.

The canonical HIF1α ubiquitination and proteasomal degradation pathway require oxygen-dependent PHD (prolyl hydroxyl domain) enzymes to hydroxylate HIF1α which then allows the E3 ligase VHL (Von Hippel-Lindau) to ubiquitinate HIF1α.[29,30] To determine whether the canonical HIF1α degradation pathway was regulating HIF1α degradation we first measured VHL protein levels. Surprisingly, VHL protein levels were reduced in Mybpc3$^{-/-}$ (Figure 3F and 3G). We then measured in situ HIF1α–VHL protein complexes and found that HIF1α–VHL complexes were significantly reduced in Mybpc3$^{-/-}$ LV tissue (Figure 3H and 3I; Figure S3B). In addition, Phd gene expression was unchanged and the pan-PHD inhibitor molidustat did not increase HIF1α protein levels in Mybpc3$^{-/-}$ mice (Figure S3C through S3F). This data shows that the canonical oxygen-dependent PHD–VHL degradation pathway is not regulating the increased proteasomal degradation of HIF1α in the Mybpc3$^{-/-}$ LV tissue.

In addition to the oxygen-dependent canonical HIF degradation pathway, oxygen-independent noncanonical HIF degradation pathways have been identified.[31,32] The E3 ligase MDM2 (murine double minute 2) has been shown to ubiquitinate HIF1α.[33] Therefore, we wanted to determine whether MDM2 was regulating the ubiquitination of HIF1α in Mybpc3$^{-/-}$ cardiomyocytes. First, we measured MDM2 protein levels and discovered that MDM2 protein levels were increased in Mybpc3$^{-/-}$ LV tissue during the same time point (postnatal day 7) when HIF1α protein was decreased (Figure 3J and 3K). Next, we selectively reduced cardiomyocyte MDM2 levels in vivo using a transgenic strategy that used a cardiomyocyte-selective Cre line (Myh6 [myosin heavy chain 6]:Cre) (Figure 3L). This strategy successfully reduced MDM2 protein levels (Figure 3M; Figure S3M). Selective reduction of cardiomyocyte MDM2 led to the normalization of HIF1α and HIF2α protein levels in Mybpc3$^{-/-}$ LV tissue (Figure 3M; Figure S3M).

We previously discovered that Mybpc3$^{-/-}$ cardiomyocytes develop increased DNA damage and increased gene expression of MDM2 at postnatal day 25.[21] Therefore, we measured MDM2 mRNA levels at postnatal day 7 to determine if increased MDM2 gene expression was the reason for the elevated MDM2 protein levels at postnatal day 7 in Mybpc3$^{-/-}$ mice. Interestingly, we found that MDM2 mRNA was reduced in the Mybpc3$^{-/-}$ mice at postnatal day 7 but was increased at postnatal day 25 (Figure S3G). It was previously shown that MDM2 can serve as a negative regulator of its own gene expression through inhibiting p53.[34] Indeed, we detected a rebound in MDM2 mRNA levels when cardiomyocyte MDM2 protein levels were reduced in Mybpc3$^{-/-}$ mice at postnatal day 7 (Figure S3H). Likewise, MDM2 mRNA increased at postnatal day 25 when levels of MDM2 protein declined (Figure S3G and S3I). These results suggested that cardiomyocyte MDM2 gene expression was not the primary cause of increased MDM2 protein levels at postnatal day 7 and suggested that MDM2 protein stability was altered in the Mybpc3$^{-/-}$ mice. Indeed, we found that MDM2 protein ubiquitination was reduced in postnatal day 7 Mybpc3$^{-/-}$ LV tissue (Figure S3J and S3K). In addition, we found that MDM2 and MDM4 (aka MDMX) protein complexes were reduced in Mybpc3 LV tissue (Figure S3L). It was previously shown that MDM4 can stimulate MDM2 autoubiquitination and degradation.[35] Importantly, when MDM2 protein levels decrease at postnatal day 25 in the Mybpc3$^{-/-}$ mice (Figure S3I), this is associated with a normalization of myocardial levels of HIF1α and HIF2α (Figure 2A and 2B). Overall,

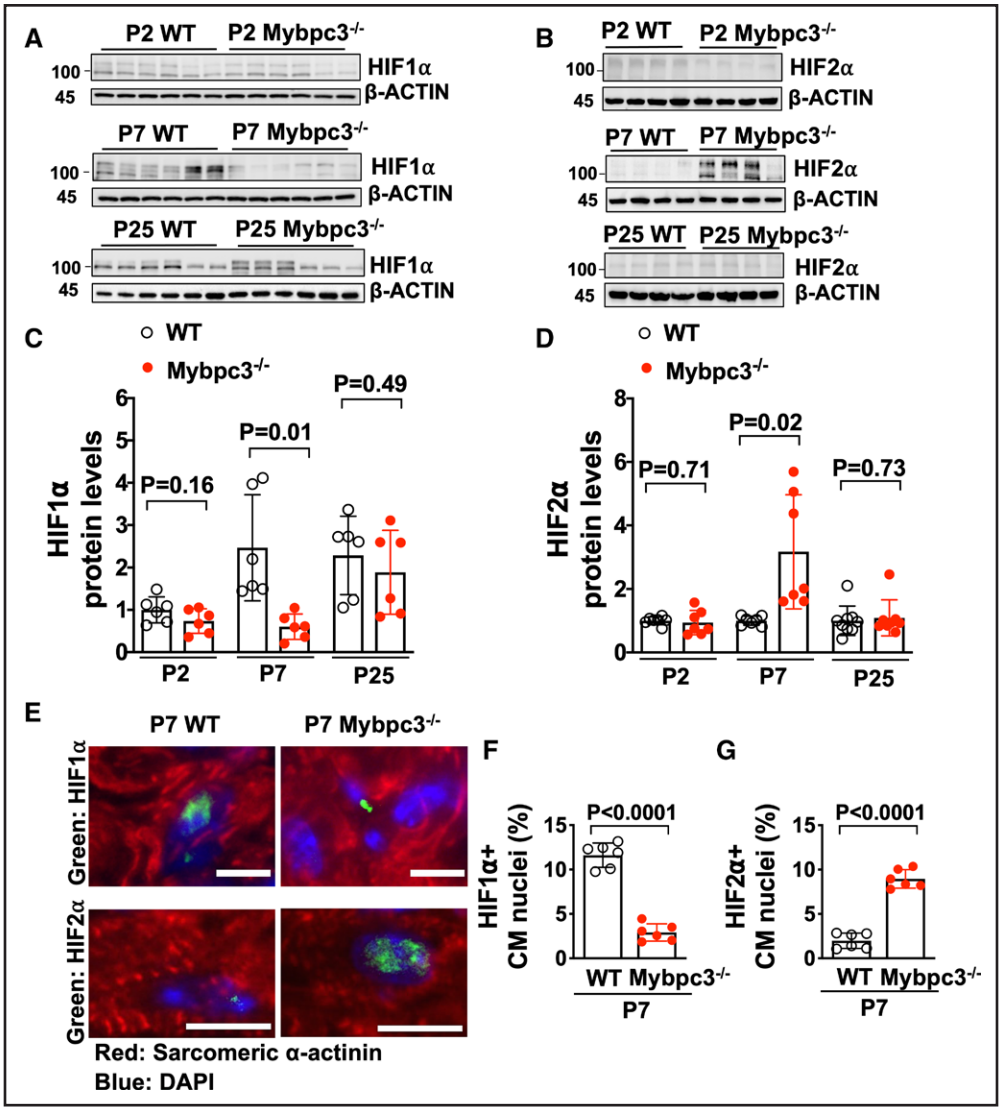

Figure 2. Dynamic changes in HIF1α and HIF2α occur during the early postnatal period in the Mybpc3$^{-/-}$ myocardium. Immunoblots for HIF1α (**A**) and HIF2α (**B**) in left ventricular tissue lysates from WT and Mybpc3$^{-/-}$ mice at postnatal day 2 (P2), postnatal day 7 (P7), or postnatal day 25 (P25). **C**, HIF1α protein quantification from WT (n=6) and Mybpc3$^{-/-}$ (n=6) left ventricular tissue lysates from P2, P7, or P25 mice normalized to β-actin protein expression and relative to postnatal day 2 WT mice. **D**, HIF2α protein quantification from WT (n=7–9) and Mybpc3$^{-/-}$ (n=7–8) left ventricular tissue from postnatal days 2, 7, or 25 mice normalized to β-actin and relative to postnatal day 2 WT mice. **E**, Representative immunohistochemistry images for HIF1α (**top**; green) and HIF2α (**bottom**; green) costained with sarcomeric α-actinin (red), in left ventricular tissue from postnatal day 7 WT and Mybpc3$^{-/-}$ mice. Nuclei are blue (DAPI); scale bars=5 um (HIF1) or 10 μm (HIF2). **F**, HIF1α-positive CM nuclei (% of total nuclei) in left ventricular tissue from postnatal day 7 WT (n=6) and Mybpc3$^{-/-}$ (n=6) mice. Minimum 100 nuclei per sample. **G**, HIF2α-positive CM nuclei (% of total nuclei) in left ventricular tissue from postnatal day 7 WT (n=6) and Mybpc3$^{-/-}$ (n=6) mice. Minimum 100 nuclei per sample. All results are shown as mean±SEM; Student or Welch *t* test were used for **C**, **D**, **F**, and **G**. CM indicates cardiomyocyte; DAPI, 4′,6-diamidino-2-phenylindole; HIF1α, hypoxia-inducible factor 1 alpha; HIF2α, hypoxia-inducible factor 2 alpha; Mybpc3$^{-/-}$, cardiac myosin binding protein 3 homozygous deletion; and WT, wild-type.

these results suggest that MDM2 protein is increased at postnatal day 7 in the Mybpc3$^{-/-}$ myocardium secondary changes in its protein stability.

Next, we measured in situ HIF1α-MDM2 protein complexes and discovered that they were robustly increased in Mybpc3$^{-/-}$ LV tissue and greatly reduced by selective cardiomyocyte reduction of MDM2 (Figure 3N and 3O; Figure S3N). We then measured in situ HIF1α ubiquitination in LV tissue and found that a reduction of cardiomyocyte MDM2 led to a corresponding reduction in HIF1α ubiquitination (Figure 3P and 3Q). We confirmed our in situ proximity ligation assay results by performing immunoprecipitation of LV tissue lysates using a HIF1α antibody and then immunoblotting with a K48 ubiquitin selective antibody (Figure 3R). Finally, the E3 ligase function of MDM2 is a well-described inducer of p53 protein degradation.[36] Therefore, we wanted to determine whether reducing cardiomyocyte MDM2 led to a surge of p53 protein levels. However, this did not occur, and LV p53 protein levels decreased in parallel with a

ORIGINAL RESEARCH ARTICLE

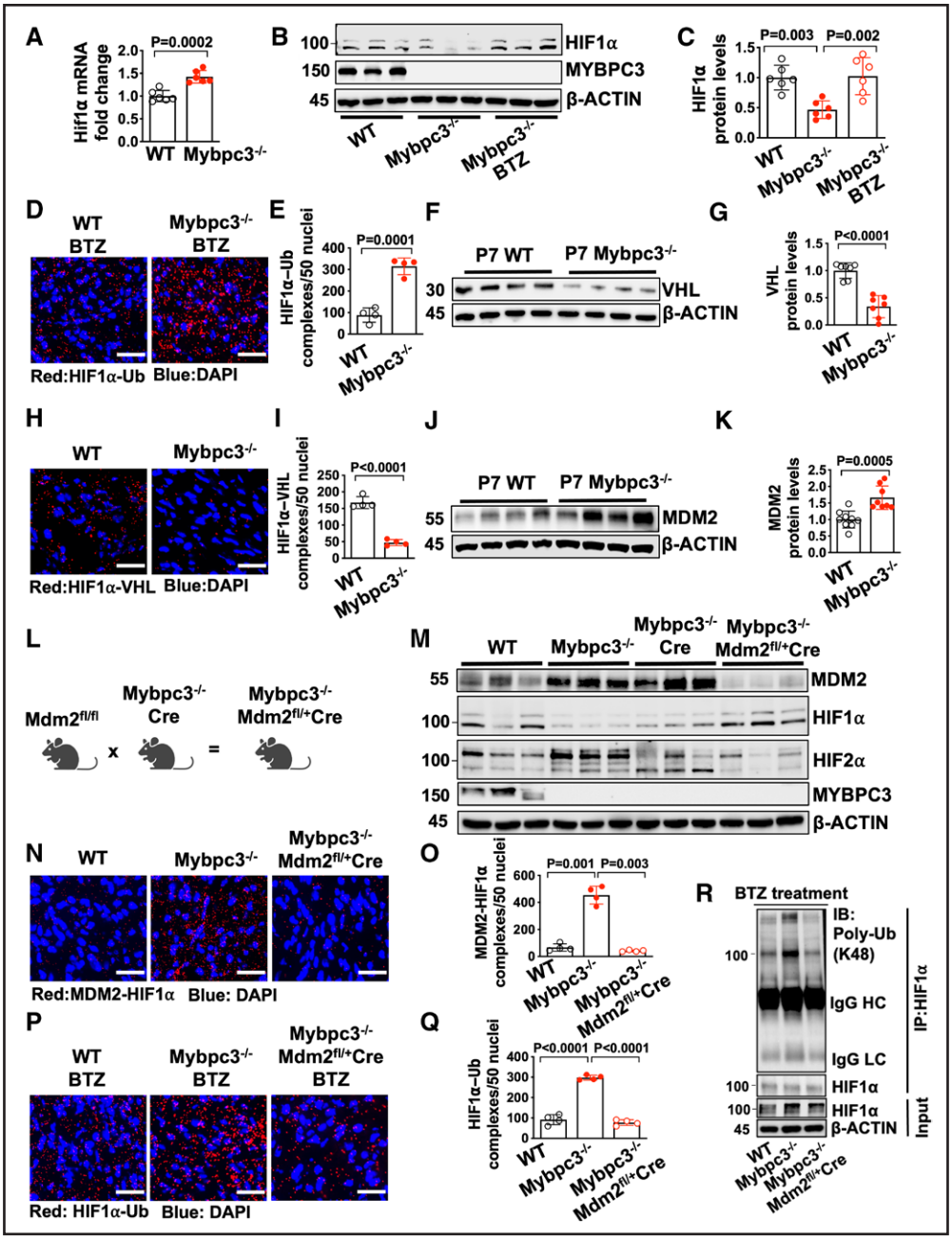

Figure 3. The noncanonical degradation of HIF1α in the Mybpc3$^{-/-}$ myocardium is regulated by cardiomyocyte MDM2.
A, *Hif1α* gene expression in left ventricular tissue RNA from postnatal day 7 (P7) WT (n=6) and Mybpc3$^{-/-}$ (n=6) mice. *Hif1α* gene expression was normalized to *Rpl32* and fold change relative to WT. **B** and **C**, Immunoblots and protein quantification for HIF1α in left ventricular tissue lysates from P7 WT (n=6), Mybpc3$^{-/-}$ (n=6), and BTZ-injected Mybpc3$^{-/-}$ (n=6) mice normalized to β-actin and relative to WT. **D** and **E**, Representative in situ proximity ligation assay images and quantification for Ub-modified HIF1α in left ventricular tissue from BTZ injected P7 WT (n=4) and Mybpc3$^{-/-}$ (n=4) mice. HIF1α–Ub complexes are red and nuclei are blue (DAPI). Three nonoverlapping left ventricular images per sample; scale bars=25 μm. **F** and **G**, Immunoblot and quantification for VHL in left ventricular tissue lysate from P7 WT (n=7) and Mybpc3$^{-/-}$ (n=7) mice normalized to beta-actin and relative to WT. **H** and **I**, Representative in situ proximity ligation assay images and quantification for HIF1α and VHL protein complexes in left ventricular tissue from P7 WT (n=4) and Mybpc3$^{-/-}$ (n=4) mice. HIF1α–VHL complexes are shown in red and nuclei are blue (DAPI); 3 nonoverlapping left ventricular images per sample; scale bars=25 μm. **J** and **K**, Immunoblot and quantification for MDM2 in left ventricular tissue from P7 WT (n=9) and Mybpc3$^{-/-}$ (n=8) mice normalized to β-actin and relative to WT. **L**, Schematic of cardiomyocyte selective reduction of MDM2 in Mybpc3$^{-/-}$ mice generated by crossing Mdm2$^{fl/fl}$, Mybpc3$^{-/-}$, and Myh6:Cre mouse lines to create Mybpc3$^{-/-}$Mdm2$^{fl/+}$/Myh6:Cre. **M**, Immunoblot for MDM2, HIF1α, HIF2α, MYPBC3, and β-actin in left ventricular tissue from P7 WT, Mybpc3$^{-/-}$, Mybpc3$^{-/-}$/Myh6:Cre, and Mybpc3$^{-/-}$Mdm2$^{fl/+}$/Myh6:Cre mice. **N** and **O**, Representative in situ proximity ligation assay images and quantification for MDM2 and HIF1α protein complexes in left ventricular tissue from P7 WT (n=4), Mybpc3$^{-/-}$ (n=4), and Mybpc3$^{-/-}$Mdm2$^{fl/+}$/Myh6:Cre (n=4) mice. MDM2–HIF1α complexes are shown in red and nuclei are blue (DAPI). Three nonoverlapping left ventricular images per sample; scale bars=25 μm. **P** and **Q**, Representative in situ proximity ligation assay images and quantification for Ub-modified HIF1α in (*Continued*)

Figure 3 Continued. left ventricular tissue from BTZ-injected P7 WT (n=4), Mybpc3$^{-/-}$ (n=4), and Mybpc3$^{-/-}$Mdm2$^{fl/+}$/Myh6:Cre (n=4) mice. HIF1α–Ub complexes are red and nuclei are blue (DAPI). Three nonoverlapping left ventricular images per sample; scale bars=25 μm. **R**, Immunoprecipitation (IP) for HIF1α was performed on left ventricular tissue lysates from BTZ-injected P7 WT, Mybpc3$^{-/-}$ and Mybpc3$^{-/-}$Mdm2$^{fl/+}$/Myh6:Cre mice and then immunoblots were performed for K48-linked Ub and HIF1α. The input left ventricular tissue lysates also underwent immunoblotting for HIF1α and β-actin. All results are shown as mean±SEM. Student *t* test was used for **A**, **E**, **G**, **I**, and **K**; 1-way ANOVA with Tukey or Dunnett T3 multiple comparison test were used for **C**, **O**, and **Q**. BTZ indicates bortezomib; DAPI, 4′,6-diamidino-2-phenylindole; HC, heavy chain; HIF1α, hypoxia-inducible factor 1 alpha; HIF2α, hypoxia-inducible factor 2 alpha; IB, immunoblot; LC, light chain; MDM2, murine double minute 2; Mdm2$^{fl/+}$, Mdm2 heterozygous floxed; Mybpc3$^{-/-}$, cardiac myosin binding protein 3 homozygous deletion; Myh6:Cre, myosin heavy chain 6:Cre recombinase; Poly-Ub, K48-linked ubiquitin; Rpl32, ribosomal protein L32; Ub, Ubiquitin; VHL, Von Hippel-Lindau; and WT, wild-type.

reduction of cardiomyocyte MDM2 protein (Figure S3O). Overall, these results show that cardiomyocyte MDM2 is facilitating the noncanonical ubiquitination and degradation of HIF1α in Mybpc3$^{-/-}$ LV tissue.

Increased HIF2α in the Mybpc3$^{-/-}$ Myocardium Occurs Secondary to MDM2 Facilitated Degradation of VHL

Although we identified the molecular mechanisms regulating the increased degradation of HIF1α in Mybpc3$^{-/-}$ cardiomyocytes, it remained unclear why HIF2α protein levels were increased. We hypothesized that the reduced VHL protein levels may be contributing to the increased levels of HIF2α (Figure 3F). We first measured *Vhl* gene expression and detected no difference between the groups (Figure 4A). This result suggested the reduction of VHL protein in Mybpc3$^{-/-}$ LV tissue was secondary to increased proteasomal degradation. Indeed, we found that VHL protein levels rebounded to normal levels when a proteasome inhibitor was administered to the Mybpc3$^{-/-}$ mice (Figure 4B and 4C). Next, we performed a coimmunoprecipitation assay to determine whether MDM2 bound to VHL and discovered that there was increased VHL binding to MDM2 in Mybpc3$^{-/-}$ LV tissue lysates (Figure 4D). In situ MDM2–VHL protein complexes were also increased in Mybpc3$^{-/-}$ LV tissue and were reduced with the selective reduction of cardiomyocyte MDM2 (Figure 4E and 4F; Figure S4A). Next, we discovered that in situ VHL ubiquitination was increased in Mybpc3$^{-/-}$ LV tissue and this increase was eliminated with reduction of cardiomyocyte MDM2. (Figure 4G and 4H; Figure S4B). We confirmed our in situ proximity ligation assay results by performing immunoprecipitation of LV tissue lysates using a VHL antibody and then immunoblotting with a K48 ubiquitin selective antibody (Figure 4I). In contrast to VHL ubiquitination, the neddylation of VHL was unchanged (Figure S4C and S4D). Taken together, these results show that MDM2 regulates the ubiquitination and degradation of VHL in Mybpc3$^{-/-}$ cardiomyocytes.

We identified a novel role for cardiomyocyte MDM2 in the regulation of VHL ubiquitination and VHL protein stability. Therefore, we hypothesized that the increase in HIF2α protein levels in Mybpc3$^{-/-}$ LV tissue was related to the changes we identified in VHL. First, we confirmed that *Hif2α* expression was unchanged in the groups (Figure 4J). However, in situ VHL-HIF2α protein complexes were greatly reduced in the Mybpc3$^{-/-}$ LV tissue but were normalized with the reduction of MDM2 (Figure 4K and 4L; Figure S4E). Importantly, we confirmed that there were minimal MDM2 and HIF2α protein complexes in LV tissue (Figure S4F and S4G). We then measured in situ HIF2α ubiquitination and found that HIF2α ubiquitination was reduced in Mybpc3$^{-/-}$ LV tissue and was normalized by the cardiomyocyte selective reduction of MDM2 (Figure 4M and 4N; Figure S4H). Again, we confirmed our in situ proximity ligation assay results by performing immunoprecipitation of LV tissue lysates using a HIF2α antibody and then immunoblotting with a K48 ubiquitin selective antibody (Figure 4O). Overall, these results show that cardiomyocyte MDM2 facilitates the degradation of VHL which leads to dynamic increases in HIF2α protein levels.

Reduction of Cardiomyocyte MDM2 in Mybpc3$^{-/-}$ Mice Increases Myocardial Capillary Formation and Proangiogenic Gene Expression

We identified a role for cardiomyocyte MDM2 in regulating the protein stability of both HIF1α and HIF2α. Therefore, we wanted to determine whether selective reduction of cardiomyocyte MDM2 would impact capillary formation in Mybpc3$^{-/-}$ mice. Indeed, we found that the reduction of cardiomyocyte MDM2 led to increased LV capillaries in Mybpc3$^{-/-}$ mice (Figure 5A and 5B). Likewise, pericytes were also increased with selective reduction of cardiomyocyte MDM2 in Mybpc3$^{-/-}$ mice (Figure S5A and S5B). We wanted to determine whether the reduction of LV capillary density in the Mybpc3$^{-/-}$ myocardium was associated with reduced expression of angiogenic genes. Indeed, we found that Mybpc3$^{-/-}$ LV tissue had reduced expression of multiple proangiogenic genes (Figure 5C). Importantly, the selective cardiomyocyte reduction of MDM2 could reverse these gene expression changes (Figure 5C).

We next investigated whether reduction of capillary density in the Mybpc3$^{-/-}$ myocardium was secondary to the reduction of HIF1α or the increase of HIF2α protein at postnatal day 7. Selective reduction of cardiomyocyte HIF1α during the postnatal day 2 to postnatal day 7 postnatal time period in WT mice led to a reduction in LV capillary formation (Figure 5D and 5E; Figure S5C).

ORIGINAL RESEARCH ARTICLE

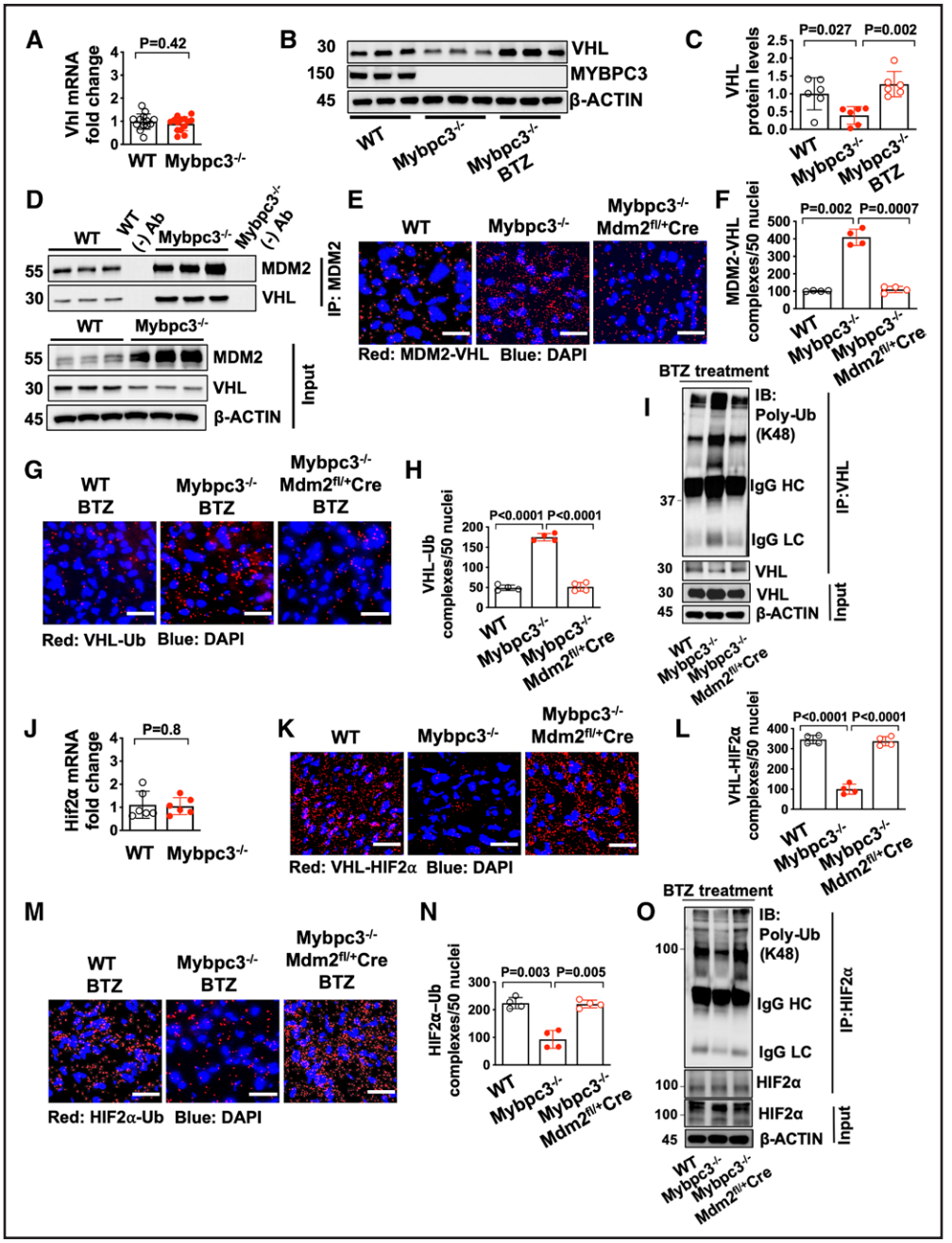

Figure 4. Increased HIF2α in the Mybpc3$^{-/-}$ myocardium occurs secondary to MDM2 facilitated degradation of VHL.
A, *Vhl*gene expression in left ventricular tissue RNA from postnatal day 7 (P7) WT (n=14) and Mybpc3$^{-/-}$ (n=14) mice. *Vhl* gene expression was normalized to *Rpl32* expression and fold-change is relative to WT. **B** and **C**, Immunoblots and protein quantification for VHL in left ventricular tissue from P7 WT (n=6), Mybpc3$^{-/-}$ (n=6) and BTZ-injected Mybpc3$^{-/-}$ (n=6) mice normalized to β-actin and relative to WT. **D**, Coimmunoprecipitation for MDM2 was performed in left ventricular tissue lysates from P7 WT and Mybpc3$^{-/-}$ mice and then immunoblots were performed for VHL and MDM2. The third WT sample (WT(-)Ab) and the third Mybpc3$^{-/-}$ sample (Mybpc3$^{-/-}$ (-) Ab) also underwent bead only precipitation without the MDM2 antibody as a negative control experiment (WT (-) Ab and Mybpc3$^{-/-}$ (-) Ab). The input left ventricular tissue lysates also underwent immunoblotting for MDM2, VHL, and β-actin. **E** and **F**, Representative in situ proximity ligation assay images and quantification for MDM2 and VHL protein complexes in left ventricular tissue from P7 WT (n=4), Mybpc3$^{-/-}$ (n=4), and Mybpc3$^{-/-}$Mdm2$^{fl/+}$/Myh6:Cre (n=4) mice. MDM2–VHL complexes are red and nuclei are blue (DAPI). Three nonoverlapping left ventricular images per sample; scale bars=25 μm. **G** and **H**, Representative in situ proximity ligation assay images and quantification for Ub-modified VHL in left ventricular tissue from BTZ-treated P7 WT (n=4), Mybpc3$^{-/-}$ (n=4), and Mybpc3$^{-/-}$Mdm2$^{fl/+}$/Myh6:Cre (n=4) mice. VHL–Ub complexes are red and nuclei are blue (DAPI). Three nonoverlapping left ventricular images per sample; scale bars=25 μm. **I**, Immunoprecipitation (IP) for VHL was performed on left ventricular tissue lysates from BTZ-injected P7 WT, Mybpc3$^{-/-}$ and Mybpc3$^{-/-}$Mdm2$^{fl/+}$/Myh6:Cre mice and then immunoblots were performed Poly-Ub and VHL. The input left ventricular tissue lysates also underwent immunoblotting for VHL and β-actin. **J**, *Hif2α* gene expression in left ventricular tissue RNA from P7 WT (n=6) and Mybpc3$^{-/-}$ (n=6) mice. *Hif2α* gene expression was normalized to *Rpl32* and fold change is relative to WT. **K** and **L**, Representative in situ proximity ligation assay images for VHL and HIF2α protein complexes in left ventricular (*Continued*)

Figure 4 Continued. tissue from P7 WT (n=4), Mybpc3$^{-/-}$ (n=4), and Mybpc3$^{-/-}$Mdm2$^{fl/+}$/Myh6:Cre (n=4) mice. VHL–HIF2α complexes are red and nuclei are blue (DAPI). Three nonoverlapping left ventricular images per sample; scale bars=25 μm. **M** and **N**, Representative in situ proximity ligation assay images and quantification for Ub-modified HIF2α in left ventricular tissue from BTZ-injected P7 WT (n=4), Mybpc3$^{-/-}$ (n=4), and Mybpc3$^{-/-}$Mdm2$^{fl/+}$/Myh6:Cre (n=4) mice. HIF2α–Ub complexes are red and nuclei are blue (DAPI). Three nonoverlapping left ventricular images per sample; scale bars=25 μm. **O**, IP for HIF2α was performed on left ventricular tissue lysates from BTZ-injected P7 WT, Mybpc3$^{-/-}$, and Mybpc3$^{-/-}$Mdm2$^{fl/+}$/Myh6:Cre mice, and then immunoblots for Poly–Ub and HIF2α. The input left ventricular tissue lysates also underwent immunoblotting for HIF2α and β-actin. All results are shown as mean±SEM. Student *t* test was used for **A** and **J**; 1-way ANOVA with Tukey or Dunnett T3 multiple comparison test were used for **C**, **F**, **H**, **L**, and **N**. BTZ indicates bortezomib; DAPI, 4′,6-diamidino-2-phenylindole; HC, heavy chain; HIF1α, hypoxia-inducible factor 1 alpha; HIF2α, hypoxia-inducible factor 2 alpha; IB, immunoblot; LC, light chain; MDM2, murine double minute 2; Mdm2$^{fl/+}$, Mdm2 heterozygous floxed; Mybpc3$^{-/-}$, cardiac myosin binding protein 3 homozygous deletion; Myh6:Cre, myosin heavy chain 6:Cre recombinase; Poly-Ub, K48-linked ubiquitin; Ub, Ubiquitin; VHL, Von Hippel-Lindau; and WT, wild-type.

In contrast, the reduction of cardiomyocyte HIF2α in Mybpc3$^{-/-}$ mice resulted in a partial increase of capillary density in Mybpc3$^{-/-}$ mice but had no impact on WT LV capillary density (Figure 5G and 5H; Figure S5D). These results show that the transient imbalance of both HIF1α and HIF2α are contributing to the capillary formation abnormality in Mybpc3$^{-/-}$ mice.

Mybpc3$^{-/-}$ mice rapidly develop LVH and LV dysfunction in the early postnatal time period.[20] Therefore, we measured cardiac structure and function in Mybpc3$^{-/-}$ mice with reduction of cardiomyocyte MDM2. We discovered that selective reduction of cardiomyocyte MDM2 did reduce LVH and improve systolic function in Mybpc3$^{-/-}$ mice during the early postnatal time period (Figure S5E through S5G). In contrast, targeted elimination of cardiomyocyte HIF1α and HIF2α did not cause significant changes in cardiac structure or function in the early postnatal time period (Figure S5H through S5M). These results show that the MDM2-induced HIF imbalance selectively alters LV capillary formation during the early postnatal time period in Mybpc3$^{-/-}$ mice.

MDM2 Regulates Capillary Formation Before the Development of Ventricular Hypertrophy in Myh6$^{R404Q/WT}$ Mice

We discovered that Mybpc3$^{-/-}$ mice have reduced LV capillary formation during the early postnatal time period and that MDM2 plays a critical role in this process. However, it remained unclear whether LV capillary formation defects could occur independently of LVH and whether other sarcomere gene mutations had shared pathophysiologic responses to the Mybpc3$^{-/-}$ mice. To address these questions, we used genetic editing to create a murine model with a point mutation in the *Myh6* gene (Myh6$^{R404Q/WT}$) (Figure S6A and S6B) to model the human *MYH7* R403Q mutation, which is a well described cause of HCM in humans.[37] The murine MYH6 protein is targeted because it is the dominant myosin heavy chain protein in the adult mouse LV versus MYH7 in the adult human LV and this strategy was successfully used in the past with homologous recombination methods.[38] In contrast to Mybpc3$^{-/-}$ mice that rapidly develop LVH by postnatal day 7, heterozygote Myh6$^{R404Q/WT}$ mice had normal LV wall thickness through postnatal day 25 but developed LVH by postnatal day 60 without systolic dysfunction (Figure 6A through 6C; Figure S6C). Male and female Myh6$^{R404Q/WT}$ mice developed similar levels of LVH by postnatal day 60 but male mice had slightly more LVH by 6 months of age (Figure S6D through S6G). Similar to the development of myocardial hypertrophy, the heterozygote Myh6$^{R404Q/WT}$ mice developed cardiomyocyte hypertrophy by postnatal day 60 (Figure 6D and 6E). Therefore, this HCM model of adult onset LVH allowed us to determine whether sarcomere protein dysfunction impacted myocardial capillary formation before the development of LVH.

We analyzed LV capillary density in the Myh6$^{R404Q/WT}$ mice and discovered that capillary formation was reduced (Figure 6F through 6I, Video 3 and 4). Similar to Mybpc3$^{-/-}$ mice, both male and female Myh6$^{R404Q/WT}$ mice had similar reductions in capillary density (Figure S6H). However, in contrast to Mybpc3$^{-/-}$ mice, LCA size of Myh6$^{R404Q/WT}$ mice was similar to WT mice at postnatal day 7 (Figure S6I and S6J). We then wanted to determine whether the changes in LV capillary formation in Myh6$^{R404Q/WT}$ mice were related to changes in MDM2-HIF signaling. We found that Myh6$^{R404Q/WT}$ myocardium had an increase in MDM2 protein (Figure 6J and 6K). Similar to Mybpc3$^{-/-}$ mice,[21] the increase in MDM2 in the Myh6$^{R404Q/WT}$ mice was associated with increased cardiomyocyte DNA damage (Figure S6K and S6L). Importantly, we found no evidence of increased endothelial cell DNA damage (Figure S6M and S6N). We then measured HIF1α and HIF2α protein levels and discovered that postnatal day 7 Myh6$^{R404Q/WT}$ myocardium had reduced HIF1α and increased HIF2α protein levels (Figure 6J, 6L, and 6M). In addition, VHL protein levels were also reduced in postnatal day 7 Myh6$^{R404Q/WT}$ myocardium (Figure S6O and S6P). Next, we wanted to determine whether selective reduction of cardiomyocyte MDM2 would increase capillary density and prevent MVD in Myh6$^{R404Q/WT}$ mice in the pre-LVH period. Indeed, we found that genetic reduction of cardiomyocyte MDM2 in Myh6$^{R404Q/WT}$ mice led to increased LV capillary formation and normalization of coronary flow reserve (Figure 6N and 6O; Figure S7A through S7C). In contrast to the Mybpc3$^{-/-}$ model that had LVH at postnatal day 7, we did not detect evidence of myocardial tissue hypoxia in the

ORIGINAL RESEARCH ARTICLE

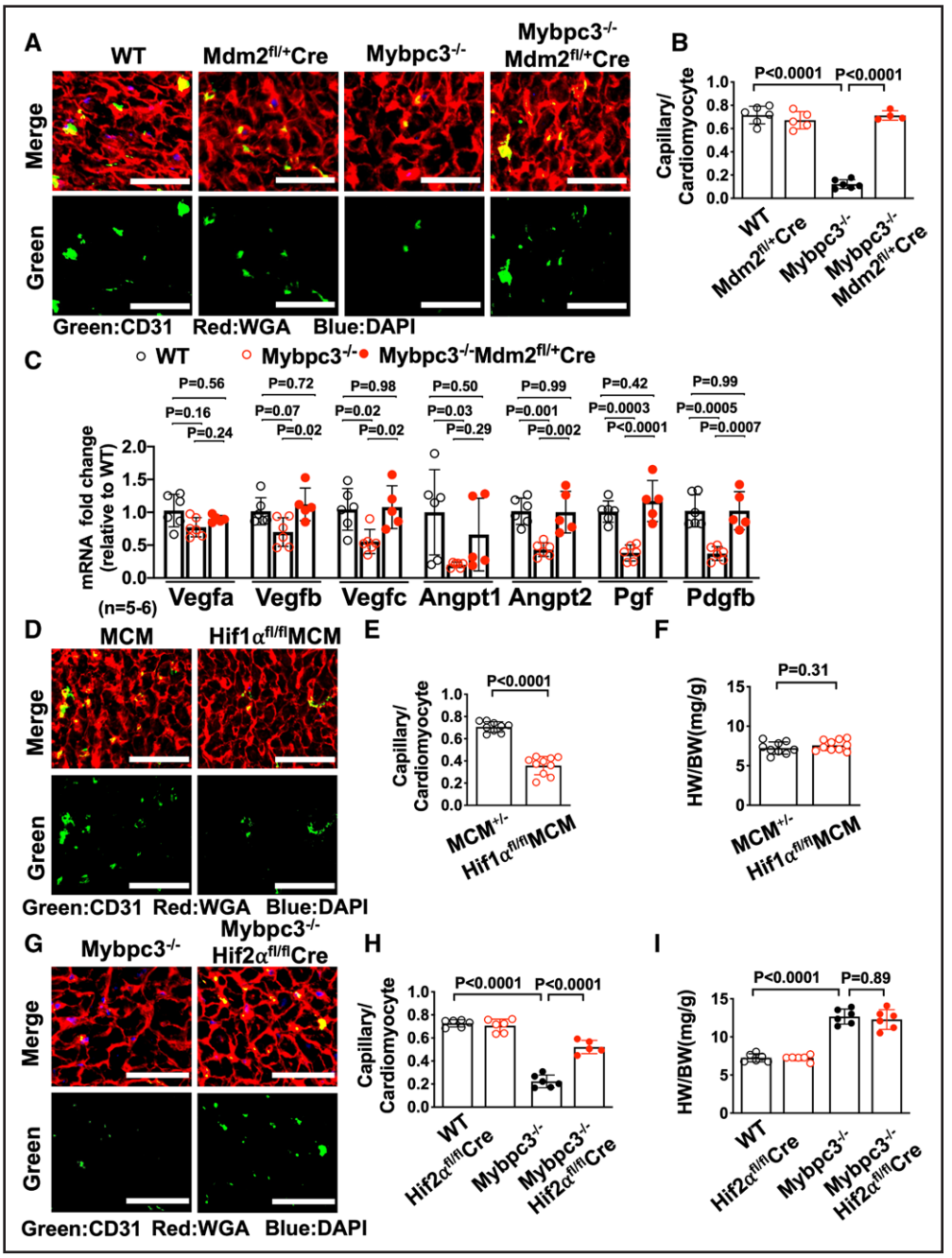

Figure 5. Reduction of cardiomyocyte MDM2 in Mybpc3$^{-/-}$ mice increases myocardial capillary formation and proangiogenic gene expression.

A, Representative immunohistochemistry images for CD31 (green) costained with WGA (red) in left ventricular tissue from postnatal day 7 (P7) WT, Mdm2$^{fl/+}$/Myh6:Cre, Mybpc3$^{-/-}$, and Mybpc3$^{-/-}$Mdm2$^{fl/+}$/Myh6:Cre mice. Nuclei are blue (DAPI); scale bars=30 µm. **B**, Capillary-to-cardiomyocyte ratios in left ventricular tissue from P7 WT (n=6), Mdm2$^{fl/+}$/Myh6:Cre (n=5), Mybpc3$^{-/-}$ (n=6), and Mybpc3$^{-/-}$ Mdm2$^{fl/+}$/Myh6:Cre (n=4) mice. Minimum 100 cardiomyocytes per sample. **C**, Proangiogenic gene expression (eg, *Vegfa*, *Vegfb*, *Vegfc* [vascular endothelial growth factor a/b/c], *Angpt1*, *Angpt2* [angiopoietin 1/2], *Pgf* [placental growth factor], *Pdgfb* [platelet-derived growth factor subunit b]) in left ventricular tissue RNA from P7 WT (n=6), Mybpc3$^{-/-}$ (n=6), and Mybpc3$^{-/-}$ Mdm2$^{fl/+}$/Myh6:Cre (n=5) mice. The genes of interest were normalized to *Rpl32* (ribosomal protein L32) and fold changes are relative to WT. **D**, Representative immunohistochemistry images for CD31 (green) costained with WGA (red) in left ventricular tissue from P7 Myh6:MerCreMer (MCM) and Hif1α$^{fl/fl}$MCM mice injected with tamoxifen at postnatal days 1 (P1) and 4 (P4). Nuclei are blue (DAPI); scale bars=50 µm. **E**, Capillary-to-cardiomyocyte ratios in left ventricular tissue from P7 MCM (n=9) and Hif1α$^{fl/fl}$MCM (n=10) injected with tamoxifen at P1 and P4. Minimum 200 cardiomyocytes per sample. **F**, Heart weight (mg)–to–body weight (g) ratios (HW/BW) from P7 MCM (n=9) and Hif1α$^{fl/fl}$ MCM (n=10) mice injected with tamoxifen at P1 and P4. **G**, Representative immunohistochemistry images for CD31 (green) costained with WGA (red) in left ventricular tissue from P7 Mybpc3$^{-/-}$ and Mybpc3$^{-/-}$Hif2α$^{fl/fl}$/Myh6:Cre mice. Nuclei are blue (DAPI). Scale bars=50 µm. **H**, Capillary-to-cardiomyocyte ratios in left ventricular tissue from P7 WT (n=6), Hif2α$^{fl/fl}$/Myh6:Cre (n=6), Mybpc3$^{-/-}$ (n=6), and Mybpc3$^{-/-}$Hif2α$^{fl/fl}$/Myh6:Cre (n=5) mice. Minimum 200 cardiomyocytes per sample. **I**, HW/BW from P7 WT (n=6), Hif2α$^{fl/fl}$/Myh6:Cre (n=6), Mybpc3$^{-/-}$ (n=6), and Mybpc3$^{-/-}$Hif2α$^{fl/fl}$/Myh6:Cre (n=6) mice. All results are shown as mean±SEM. (*Continued*)

Figure 5 Continued. Student *t* test used for **E** and **F**; 1-way ANOVA with Tukey or Dunnett T3 multiple comparison test used for **C**; 2-way ANOVA with Tukey multiple comparison test used for **B**, **H**, and **I**. CD31 indicates cluster of differentiation 31; DAPI, 4′,6-diamidino-2-phenylindole; HIF1α, hypoxia-inducible factor 1 alpha; HIF2α, hypoxia-inducible factor 2 alpha; $Hif2\alpha^{fl/fl}$, Hif2α homozygous floxed; IB, immunoblot; MDM2, murine double minute 2; $Mdm2^{fl/+}$, Mdm2 heterozygous floxed; MerCreMer, tamoxifen inducible Cre recombinase; $Mybpc3^{-/-}$, cardiac myosin binding protein 3 homozygous deletion; WGA, wheat germ agglutinin; and WT, wild-type.

$Myh6^{R404Q/WT}$ model at postnatal day 7 (Figure S7D). Therefore, despite the absence of myocardial tissue hypoxia in the $Myh6^{R404Q/WT}$ model, the abnormalities in the microvasculature and molecular alterations in MDM2, HIF1/2, and VHL were conserved with the $Mybpc3^{-/-}$ model. Overall, these results show that myocardial capillary formation precedes the development of ventricular hypertrophy in $Myh6^{R404Q/WT}$ mice and MVD can be prevented by genetic reduction of cardiomyocyte MDM2.

Chemical Inhibition of MDM2 Prevents MVD in Two Distinct HCM Models

We discovered that cardiomyocyte MDM2 regulates the development of MVD in both the $Mybpc3^{-/-}$ and $Myh6^{R404Q/WT}$ mouse lines. Therefore, we wanted to determine whether chemically targeting MDM2 could prevent the development of MVD in these models. We used MD-224, a chemical proteolysis targeting chimeric compound, to selectively degrade MDM2 in the early postnatal time period (Figure 7A). Chemical targeting of MDM2 led to the normalization of HIF1α and HIF2α levels in both $Mybpc3^{-/-}$ (Figure 7B) and $Myh6^{R404Q/WT}$ mice (Figure 7C). Likewise, chemical MDM2 degradation led to an increase in LV capillary density in both $Mybpc3^{-/-}$ and $Myh6^{R404Q/WT}$ mice (Figure 7D and 7E).

Similar to genetic reduction of MDM2, chemical targeting of MDM2 using MD-224 reduced myocardial hypertrophy and improved LV systolic function in $Mybpc3^{-/-}$ mice (Figure S8A through S8F). Next, we wanted to determine whether transient targeting of MDM2 during the prehypertrophic period of $Myh6^{R404Q/WT}$ mice would lead to persistent improvement in LV capillary density and coronary flow reserve in the adult animal (Figure 7F). We found that transient chemical targeting of MDM2 during the early postnatal time period led to a persistent increase in LV capillary density and normalized coronary flow reserve in adult $Myh6^{R404Q/WT}$ mice (Figure 7G through 7I; Figure S8G). In addition, transient chemical targeting of MDM2 prevented the development of LVH in the $Myh6^{R404Q/WT}$ model at postnatal day 60 (Figure S8H through S8M). In summary, these findings show that transient chemical targeting of MDM2 prevents the HIF imbalance and myocardial capillary dysfunction in 2 unrelated models of HCM.

DISCUSSION

Myocardial MVD has been identified in multiple different forms of human cardiomyopathy and is often thought to occur as a consequence of the pathologic myocardial remodeling process.[39] Myocardial MVD has been demonstrated in humans with hypertrophic cardiomyopathy (HCM) and is thought to be a significant contributor to disease pathogenesis.[40–42] However, it remains unclear when MVD develops in HCM and the molecular mechanisms regulating this pathologic process. Using 2 distinct animal models of HCM, we discovered that early postnatal myocardial capillary formation is impaired, and this leads to MVD in adult animals. The reduction in myocardial capillary formation in HCM is caused by the E3 ligase MDM2 inducing an imbalance of cardiomyocyte HIF1α and HIF2α protein levels during the early postnatal time period. Importantly, myocardial MVD can precede the development of myocardial hypertrophy in HCM and selective targeting of MDM2 prevents myocardial MVD from developing. This study identified a key regulatory mechanism controlling the development of myocardial MVD and provides unique insights into molecular pathways contributing to the pathophysiology of HCM (Figure S9).

We have identified a unique role for MDM2 as a critical regulator of MVD in HCM by reducing myocardial angiogenesis in the early postnatal heart. MDM2 has not been previously shown to regulate MVD in the heart or other organ systems. In contrast, increased expression of MDM2 has been shown to play a proangiogenic role in malignant tissues.[43–45] The divergent pro- and antiangiogenic properties of MDM2 appear to be partially explained by the acute versus chronic overexpression of the protein. For example, the chronic overexpression of MDM2 in malignant tissues can lead to increased p53 degradation which facilitates proangiogenic gene expression.[43] In contrast, the acute increase in cardiomyocyte MDM2 in our HCM models led to an antiangiogenic role for this protein through its role in simultaneously regulating the protein stability of HIF1α and HIF2α.

We found that MDM2 concurrently regulated the noncanonical degradation of HIF1α and the canonical degradation of HIF2α leading to an imbalance in these proteins. Previously it was shown that MDM2 can regulate HIF1α ubiquitination in cancer cell lines,[31] but our data indicates this noncanonical mechanism of HIF1α degradation is important in vivo in a nonmalignant context. In addition, we discovered that in-vivo cardiomyocyte MDM2 can bind and regulate the ubiquitination of VHL leading to a reduction in the canonical degradation of HIF2α. Our results identified MDM2 as a specific regulator of HIF and VHL protein stability in the early stages of HCM and reinforces the increasing evidence that the ubiquitin–proteosome system is an important regulator in HCM.[46–49] Interestingly,

ORIGINAL RESEARCH ARTICLE

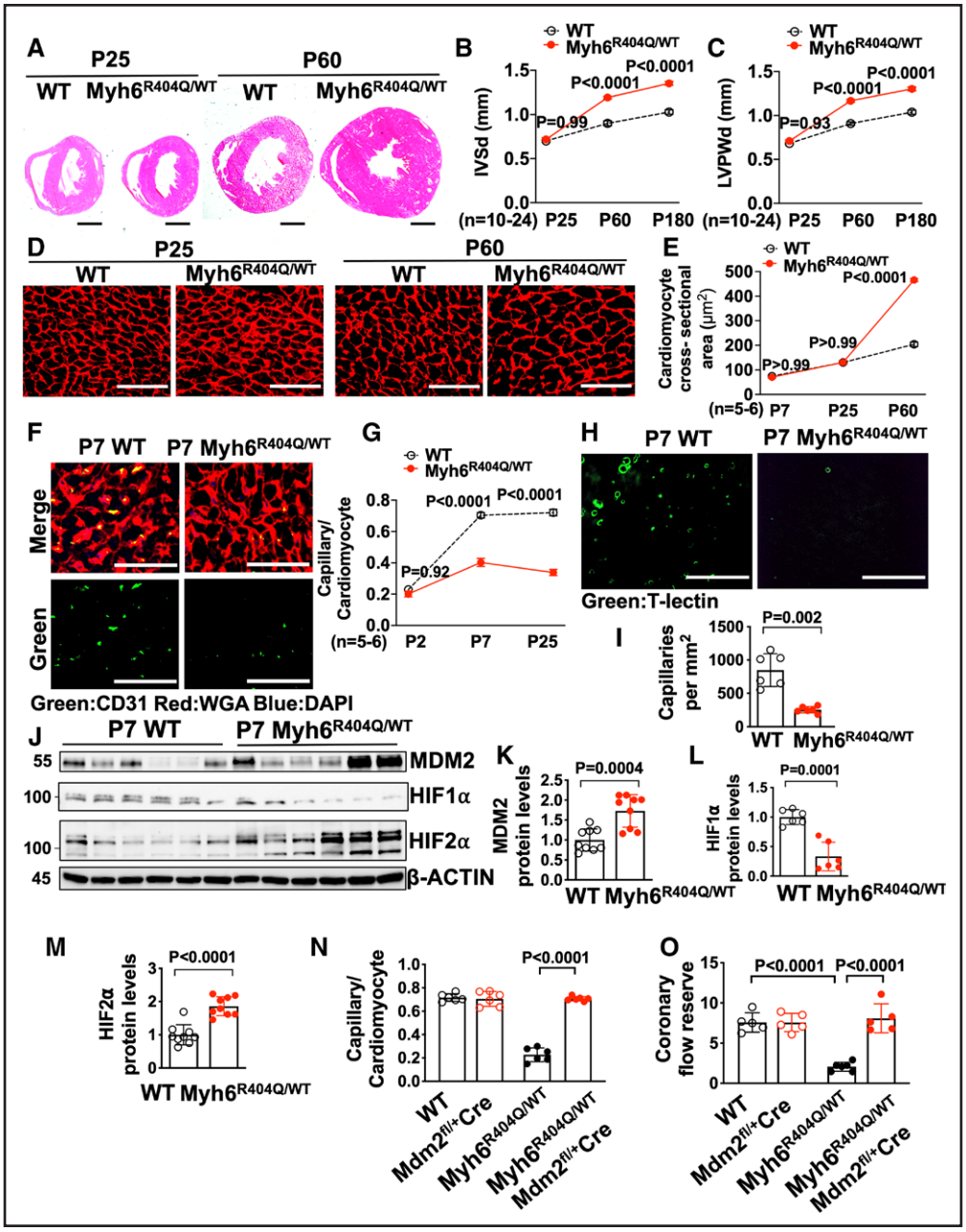

Figure 6. MDM2 regulates capillary formation in Myh6$^{R404Q/WT}$ mice before the development of ventricular hypertrophy.
A, Representative hematoxylin-eosin–stained heart cross-sections of postnatal days 25 (P25) and 60 (P60) WT and Myh6$^{R404Q/WT}$ mice. Scale bars=1 mm. Echocardiography assessment of (**B**) interventricular septal thickness at end diastole (IVSd) and (**C**) left ventricular posterior wall thickness at end diastole (LVPWd) in WT (n=10–11) and Myh6$^{R404Q/WT}$ (n=19–24) mice at P25, P60, or postnatal day 180 (P180). **D**, Representative images of WGA (red)–stained left ventricular tissue from WT and Myh6$^{R404Q/WT}$ mice at P25 or P60. Scale bar=75 μm. **E**, Cardiomyocyte cross-sectional areas from WGA-stained left ventricular tissue from WT (n=5–6) and Myh6$^{R404Q/WT}$ (n=5–6) mice at postnatal day 7 (P7), P25, or P60. Minimum 50 cardiomyocytes per sample. **F**, Representative immunohistochemistry images for CD31 (green) costained with WGA (red) in left ventricular tissue from P7 WT and Myh6$^{R404Q/WT}$ mice. Nuclei are blue (DAPI). Scale bars=50 μm. **G**, Capillary-to-cardiomyocyte ratios in left ventricular tissue from WT (n=5–6) and Myh6$^{R404Q/WT}$ (n=5–6) mice at postnatal day 2, P7, or P25. Minimum 200 cardiomyocytes per sample. **H**, Representative fluorescence images for the intravascularly injected endothelial cell stain T-lectin (green) in left ventricular tissue from P7 WT and Myh6$^{R404Q/WT}$ mice. Scale bars=80 μm. **I**, Capillaries per mm^2 in left ventricular tissue from P7 WT (n=6) and Myh6$^{R404Q/WT}$ (n=6) mice; 3 cross-sectional images per sample were analyzed. **J** through **M**, Immunoblots and quantification for MDM2, HIF1α, and HIF2α in left ventricular tissue lysates from P7 WT (n=6–9) and Myh6$^{R404Q/WT}$ (n=6–9) mice normalized to β-actin and relative to WT. **N**, Capillary-to-cardiomyocyte ratios were calculated from left ventricular tissue in P7 WT (n=6), Mdm2$^{fl/+}$/Myh6:Cre (n=6), Myh6$^{R404Q/WT}$ (n=6), and Myh6$^{R404Q/WT}$Mdm2$^{fl/+}$/Myh6:Cre (n=6) mice. Minimum 200 cardiomyocytes per sample. **O**, Coronary flow reserve in P25 WT (n=5), Mdm2$^{fl/+}$/Myh6:Cre (n=5), Myh6$^{R404Q/WT}$ (n=6), and Myh6$^{R404Q/WT}$Mdm2$^{fl/+}$/Myh6:Cre (n=5) mice. All results are shown as mean±SEM. Student or Welch *t* test used for **I**, **K**, **L**, and **M**; 2-way ANOVA with Tukey multiple comparison test used for **B**, **C**, **E**, **G**, **N**, and **O**. CD31 indicates cluster of differentiation 31; DAPI, 4′,6-diamidino-2-phenylindole; HIF1α, hypoxia-inducible factor 1 alpha; HIF2α, hypoxia-inducible factor 2 alpha; MDM2, murine double minute 2; Mdm2$^{fl/+}$Cre, Mdm2 heterozygous floxed and Myh6:Cre; Mybpc3$^{-/-}$ cardiac myosin binding protein 3 homozygous deletion; Myh6:Cre, myosin heavy chain 6:Cre recombinase; Myh6$^{R404Q/WT}$, myosin heavy chain 6 arginine to glutamine substitution at amino acid 404 heterozygous; T-lectin, tomato lectin; WGA, wheat germ agglutinin; and WT, wild-type.

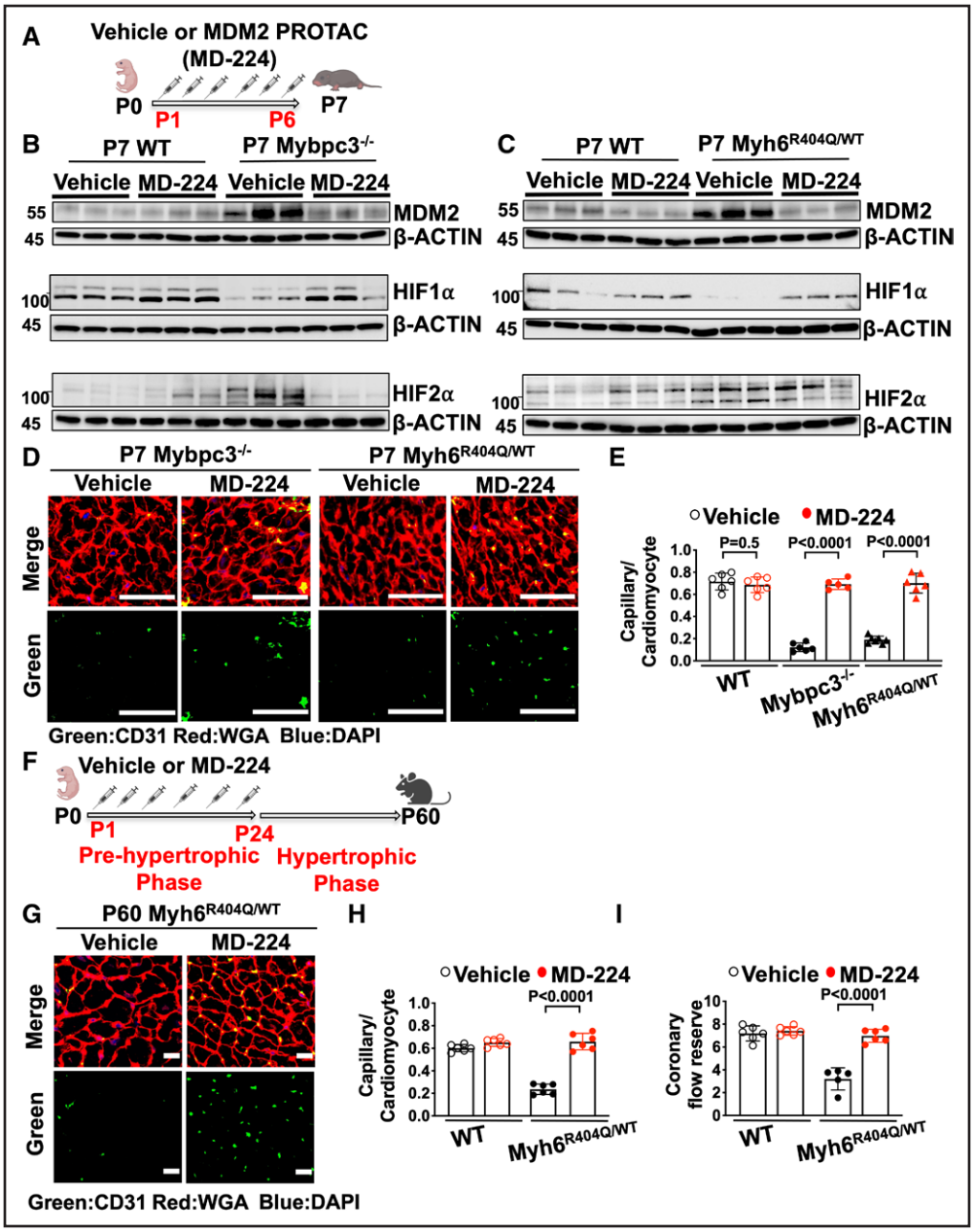

Figure 7. Chemical inhibition of MDM2 prevents microvascular dysfunction in 2 distinct HCM models.
A, Schematic of injections of vehicle or MDM2 PROTAC (MD-224) from postnatal days 1 (P1) to 6 (P6). **B**, Immunoblots for MDM2, HIF1α, and HIF2α in left ventricular tissue from postnatal day 7 (P7) WT or Mybpc3$^{-/-}$ injected with vehicle or MD-224. **C**, Immunoblots for MDM2, HIF1α, and HIF2α in left ventricular tissue from P7 WT and Myh6$^{R404Q/WT}$ injected with vehicle or MD-224. **D**, Representative immunohistochemistry images for CD31 (green) costained with WGA (red) in left ventricular tissue from P7 Mybpc3$^{-/-}$ and Myh6$^{R404Q/WT}$ injected with vehicle or MD-224 from P1 to P6. Nuclei are blue (DAPI); scale bars=50 μm. **E**, Capillary-to-cardiomyocyte ratios in left ventricular tissue from P7 WT vehicle (n=6), WT MD-224 (n=6), Mybpc3$^{-/-}$ vehicle (n=6), Mybpc3$^{-/-}$ MD-224 (n=5), Myh6$^{R404Q/WT}$ vehicle (n=7), and Myh6$^{R404Q/WT}$ MD-224 (n=6) mice. All groups injected from P1 to P6 with either vehicle or MD-224. Minimum 200 cardiomyocytes per sample. **F**, Schematic of WT or Myh6$^{R404Q/WT}$ mice injected with vehicle or MDM2 PROTAC (MD-224) from P1 to postnatal day 24 (P24), and then analyzed at postnatal day 60 (P60). **G**, Representative immunohistochemistry images for CD31 (green) costained with WGA (red) in left ventricular tissue from P60 Myh6$^{R404Q/WT}$ mice injected with vehicle or MD-224 from P1 to P24. Nuclei are blue (DAPI). Scale bars=15 μm. **H**, Capillary-to-cardiomyocyte ratios in left ventricular tissue from P60 WT vehicle (n=6), WT MD-224 (n=6), Myh6$^{R404Q/WT}$ vehicle (n=6), and Myh6$^{R404Q/WT}$ MD-224 (n=6) mice. All groups injected from P1 to P24 with vehicle or MD-224. Minimum 140 cardiomyocytes per sample. **I**, Coronary flow reserve was calculated in P60 WT vehicle (n=6), WT MD-224 (n=6), Myh6$^{R404Q/WT}$ vehicle (n=5), and Myh6$^{R404Q/WT}$ MD-224 (n=6) mice. All results are shown as mean±SEM. Student or Welch *t* test used for **E**, **H**, and **I**. CD31 indicates cluster of differentiation 31; DAPI, 4′,6-diamidino-2-phenylindole; HIF1α, hypoxia-inducible factor 1 alpha; HIF2α, hypoxia-inducible factor 2 alpha; MDM2, murine double minute 2; Mybpc3$^{-/-}$, cardiac myosin binding protein 3 homozygous deletion; Myh6$^{R404Q/WT}$, myosin heavy chain 6 arginine to glutamine substitution at amino acid 404 heterozygous; PROTAC, proteolysis targeting chimera; WGA, wheat germ agglutinin; and WT, wild-type.

it was previously shown that MDM2 can also regulate VHL neddylation in cancer cell lines.[50] However, in contrast to the effect that MDM2 has on VHL ubiquitination, we found no evidence that MDM2 dynamically regulated VHL neddylation in vivo in our disease model. Interestingly, we discovered that HIF1α and HIF2α have opposing roles in regulating myocardial capillary formation in the postnatal mammalian heart, with HIF1α serving a proangiogenic role and HIF2α serving an antiangiogenic role. This is in contrast to tumor angiogenesis, where HIF1α and HIF2α are more often reported to have synergistic roles in promoting angiogenesis.[51] Our data shows that the regulation of organ angiogenesis by HIF1α and HIF2α is highly dependent on cell type and tissue environment. This study adds to the growing data that cardiomyocyte HIF signaling has distinct roles in regulating myocardial growth and maturation depending on the developmental time point when they are expressed.[52,53]

Another important result from this study is that MVD can develop before cardiomyocyte hypertrophy. Using our Myh6^{R404Q} HCM model that develops LVH in the adolescent period of mouse development, we identified early postnatal capillary defects before the development of LVH. These results suggest that myocardial MVD and myocardial hypertrophy in HCM can occur through distinct molecular mechanisms. Supporting this conclusion are the results from our targeted cardiomyocyte deletion of the MDM2 target proteins HIF1α and HIF2α. Selective reduction of cardiomyocyte HIF1α and HIF2α had opposing effects on myocardial capillary growth but had no measurable impact on myocardial hypertrophic growth in the early postnatal time period. Likewise, we found that targeting MDM2 activity in the early postnatal time period in the Myh6^{R404Q} model prevented myocardial MVD well before the onset of LVH. Our results are further supported by clinical studies in human carriers of pathogenic sarcomere gene mutations which identified evidence of MVD even before the development of myocardial hypertrophy.[54–56] Although we have defined a unique role of MDM2 in regulating myocardial HIF signaling and capillary growth in 2 distinct HCM models, it remains unknown how alterations in MDM2 signaling lead to changes in cardiomyocyte hypertrophy in HCM.

In contrast to this study which is focused on how a lifelong genetic hypertrophic stimulus leads to MVD, acquired forms of LVH secondary to hypertension or aortic stenosis typically occur during adulthood. MVD in acquired forms of LVH is thought to be from capillary regression leading to microvascular rarefaction. Therefore, it would be assumed that MVD in genetic and acquired forms of hypertrophy may have divergent mechanisms. However, capillary rarefaction in pressure overload was also shown to occur before the development of LVH.[18] Likewise, alterations in p53 activity were previously identified to regulate capillary regression in a pressure overload LVH model.[16] Therefore, it will be important to determine how dynamic changes in MDM2 signaling impacts capillary rarefaction in acquired forms of LVH.

Our results show that MVD can be prevented by partial genetic or chemical reduction of MDM2 in 2 different mouse models of HCM. Importantly, we found that partial chemical or genetic reduction of MDM2 in our models did not lead to an increase in myocardial p53 protein levels. In contrast, previous studies have shown that complete ablation of cardiomyocyte MDM2 during the embryonic or adult period leads to cardiomyopathy and lethality secondary to elevated myocardial p53 levels.[57,58] Likewise, the overexpression of a negative regulator of Mdm2 mRNA stability, ZFP36L2, was found to facilitate the development of peripartum cardiomyopathy secondary to increased cardiomyocyte p53 activity leading to a reduction of mTorc1.[59] The divergent phenotypic responses in models with partial versus complete ablation of MDM2 is at least somewhat explained by these divergent p53 responses. However, the type and timing of the pathogenic stimulus may also be an important contributor.

Our data demonstrating that MDM2 regulates a critical stage of HCM disease development further reinforces that the pre- or early LVH period of HCM is important in establishing the long-term disease. We show that targeting MDM2 during this key period can modify long-term HCM pathologic remodeling. Therefore, it may be possible to target MDM2 or related pathways during the earliest stages of HCM disease development and positively impact long-term remodeling while avoiding the potential negative consequences of chronic MDM2 inhibition. The pre-LVH period in mouse HCM models is measured in days to months after birth but in humans this period is typically years in duration. Therefore, the window for targeting disease modifying pathways in human HCM may be much larger. Supporting the strategy of early disease modification in HCM was a recent clinical trial administering an angiotensin receptor blocker during the earliest stages of hypertrophic growth which successfully modified pathologic structural remodeling in HCM patients.[60]

In conclusion, our results show that sarcomere mutations cause abnormal cardiomyocyte MDM2 signaling which can occur even before the development of cardiomyocyte hypertrophy. Importantly, the early postnatal pathologic changes in cardiomyocyte MDM2 signaling led to persistent changes in the myocardial microenvironment of the adult animals. This study reinforces the importance of targeting HCM during the earliest periods of disease development in order to successfully prevent the long-term pathologic remodeling of the myocardium in this disease.

ARTICLE INFORMATION

Received February 7, 2023; accepted September 21, 2023.

Affiliations

Division of Cardiology, Department of Medicine, and Pittsburgh Heart, Lung, Blood and Vascular Medicine Institute (P.S., M.S.G., S.P., C.J.W., E.J.C., P.B., N.C.G., D.B., J.R.B.) and Department of Immunology (S.G.), University of Pittsburgh

School of Medicine and University of Pittsburgh Medical Center, PA. Department of Bioengineering, Swanson School of Engineering, University of Pittsburgh, PA (P.S., J.R.B.).

Acknowledgments

We would like to acknowledge Chunming Bi and Zhaohui Kou (Mouse Embryo Services Core, University of Pittsburgh, Department of Immunology) for microinjection of zygotes to produce the Myh6^{R404Q} founder mice.

P.S. and J.R.B. designed the research study. P.S, M.S.G., S.P, C.W., E.C., P.B., N.G.C, D.B., and J.R.B. conducted experiments and data analysis. S.G. designed the CRISPR/Cas9 vectors. P.S. and J.R.B prepared and edited the manuscript.

Sources of Funding

This work was supported by grants from the National Institutes of Health (HL136824 and HL160890 to J.R.B.). The University of Pittsburgh Small Animal Ultrasonography Core is supported by the National Institutes of Health (grant No. 1S10OD023684-01A1).

Disclosures

None.

Supplemental Material

Expanded Methods
Figures S1–S9
Tables S1–S2
Videos S1–S4
References 61–67
Uncropped Gel Blots

REFERENCES

1. Maron BJ, Bonow RO, Cannon RO, Leon MB, Epstein SE. Hypertrophic cardiomyopathy Interrelations of clinical manifestations, pathophysiology, and therapy (2). *N Engl J Med*. 1987;316:844–852. doi: 10.1056/NEJM198704023161405
2. McNally EM, Barefield DY, Puckelwartz MJ. The genetic landscape of cardiomyopathy and its role in heart failure. *Cell Metab*. 2015;21:174–182. doi: 10.1016/j.cmet.2015.01.013
3. Marian AJ, Braunwald E. Hypertrophic cardiomyopathy: genetics, pathogenesis, clinical manifestations, diagnosis, and therapy. *Circ Res*. 2017;121:749–770. doi: 10.1161/CIRCRESAHA.117.311059
4. Bos JM, Towbin JA, Ackerman MJ. Diagnostic, prognostic, and therapeutic implications of genetic testing for hypertrophic cardiomyopathy. *J Am Coll Cardiol*. 2009;54:201–211. doi: 10.1016/j.jacc.2009.02.075
5. Teekakirikul P, Eminaga S, Toka O, Alcalai R, Wang L, Wakimoto H, Nayor M, Konno T, Gorham JM, Wolf CM, et al. Cardiac fibrosis in mice with hypertrophic cardiomyopathy is mediated by non-myocyte proliferation and requires Tgf-beta. *J Clin Invest*. 2010;120:3520–3529. doi: 10.1172/JCI42028
6. Del Buono MG, Montone RA, Camilli M, Carbone S, Narula J, Lavie CJ, Niccoli G, Crea F. Coronary microvascular dysfunction across the spectrum of cardiovascular diseases: JACC State-of-the-Art Review. *J Am Coll Cardiol*. 2021;78:1352–1371. doi: 10.1016/j.jacc.2021.07.042
7. Koton S, Schneider ALC, Windham BG, Mosley TH, Gottesman RF, Coresh J. Microvascular brain disease progression and risk of stroke: the ARIC study. *Stroke*. 2020;51:3264–3270. doi: 10.1161/STROKEAHA.120.030063
8. Kang DH, Kanellis J, Hugo C, Truong L, Anderson S, Kerjaschki D, Schreiner GF, Johnson RJ. Role of the microvascular endothelium in progressive renal disease. *J Am Soc Nephrol*. 2002;13:806–816. doi: 10.1681/ASN.V133806
9. Gulati A, Ismail TF, Ali A, Hsu LY, Gonçalves C, Ismail NA, Krishnathasan K, Davendralingam N, Ferreira P, Halliday BP, et al. Microvascular dysfunction in dilated cardiomyopathy: a quantitative stress perfusion cardiovascular magnetic resonance study. *JACC Cardiovasc Imaging*. 2019;12:1699–1708. doi: 10.1016/j.jcmg.2018.10.032
10. Jia G, Hill MA, Sowers JR. Diabetic Cardiomyopathy: An Update of Mechanisms Contributing to This Clinical Entity. *Circ Res*. 2018;122:624–638. doi: 10.1161/CIRCRESAHA.117.311586
11. Crea F, Camici PG, Bairey Merz CN. Coronary microvascular dysfunction: an update. *Eur Heart J*. 2014;35:1101–1111. doi: 10.1093/eurheartj/eht513
12. Shah SJ, Lam CSP, Svedlund S, Saraste A, Hage C, Tan RS, Beussink-Nelson L, Ljung Faxén U, Fermer ML, Broberg MA, et al. Prevalence and correlates of coronary microvascular dysfunction in heart failure with preserved ejection fraction: PROMIS-HFpEF. *Eur Heart J*. 2018;39:3439–3450. doi: 10.1093/eurheartj/ehy531
13. Dorbala S, Vangala D, Bruyere J, Quarta C, Kruger J, Padera R, Foster C, Hanley M, Di Carli MF, Falk R. Coronary microvascular dysfunction is related to abnormalities in myocardial structure and function in cardiac amyloidosis. *JACC Heart Fail*. 2014;2:358–367. doi: 10.1016/j.jchf.2014.03.009
14. Singh A, Greenwood JP, Berry C, Dawson DK, Hogrefe K, Kelly DJ, Dhakshinamurthy V, Lang CC, Khoo JP, Sprigings D, et al. Comparison of exercise testing and CMR measured myocardial perfusion reserve for predicting outcome in asymptomatic aortic stenosis: the Prognostic Importance of Microvascular Dysfunction in Aortic Stenosis (PRIMID AS) study. *Eur Heart J*. 2017;38:1222–1229. doi: 10.1093/eurheartj/ehx001
15. van der Laan AM, Piek JJ, van Royen N. Targeting angiogenesis to restore the microcirculation after reperfused MI. *Nat Rev Cardiol*. 2009;6:515–523. doi: 10.1038/nrcardio.2009.103
16. Sano M, Minamino T, Toko H, Miyauchi H, Orimo M, Qin Y, Akazawa H, Tateno K, Kayama Y, Harada M, et al. p53-induced inhibition of Hif-1 causes cardiac dysfunction during pressure overload. *Nature*. 2007;446:444–448. doi: 10.1038/nature05602
17. Heineke J, Auger-Messier M, Xu J, Oka T, Sargent MA, York A, Klevitsky R, Vaikunth S, Duncan SA, Aronow BJ, et al. Cardiomyocyte GATA4 functions as a stress-responsive regulator of angiogenesis in the murine heart. *J Clin Invest*. 2007;117:3198–3210.
18. Perrino C, Naga Prasad SV, Mao L, Noma T, Yan Z, Kim HS, Smithies O, Rockman HA. Intermittent pressure overload triggers hypertrophy-independent cardiac dysfunction and vascular rarefaction. *J Clin Invest*. 2006;116:1547–1560. doi: 10.1172/JCI25397
19. Dittrich GM, Froese N, Wang X, Kroeger H, Wang H, Szaroszyk M, Malek-Mohammadi M, Cordero J, Keles M, Korf-Klingebiel M, et al. Fibroblast GATA-4 and GATA-6 promote myocardial adaptation to pressure overload by enhancing cardiac angiogenesis. *Basic Res Cardiol*. 2021;116:26. doi: 10.1007/s00395-021-00862-y
20. Nixon BR, Williams AF, Glennon MS, de Feria AE, Sebag SC, Baldwin HS, Becker JR. Alterations in sarcomere function modify the hyperplastic to hypertrophic transition phase of mammalian cardiomyocyte development. *JCI Insight*. 2017;2:e90656. doi: 10.1172/jci.insight.90656
21. Pal S, Nixon BR, Glennon MS, Shridhar P, Satterfield SL, Su YR, Becker JR. Replication stress response modifies sarcomeric cardiomyopathy remodeling. *J Am Heart Assoc*. 2021;10:e021768. doi: 10.1161/JAHA.121.021768
22. Cannon L, Yu ZY, Marciniec T, Waardenberg AJ, Iismaa SE, Nikolova-Krstevski V, Neist E, Ohanian M, Qiu MR, Rainer S, et al. Irreversible triggers for hypertrophic cardiomyopathy are established in the early postnatal period. *J Am Coll Cardiol*. 2015;65:560–569. doi: 10.1016/j.jacc.2014.10.069
23. Gedicke-Hornung C, Behrens-Gawlik V, Reischmann S, Geertz B, Stimpel D, Weinberger F, Schlossarek S, Precigout G, Braren I, Eschenhagen T, et al. Rescue of cardiomyopathy through U7snRNA-mediated exon skipping in Mybpc3-targeted knock-in mice. *EMBO Mol Med*. 2013;5:1128–1145. doi: 10.1002/emmm.201202168
24. Jiang J, Wakimoto H, Seidman JG, Seidman CE. Allele-specific silencing of mutant Myh6 transcripts in mice suppresses hypertrophic cardiomyopathy. *Science*. 2013;342:111–114. doi: 10.1126/science.1236921
25. Armulik A, Genove G, Betsholtz C. Pericytes: developmental, physiological, and pathological perspectives, problems, and promises. *Dev Cell*. 2011;21:193–215. doi: 10.1016/j.devcel.2011.07.001
26. Robertson RT, Levine ST, Haynes SM, Gutierrez P, Baratta JL, Tan Z, Longmuir KJ. Use of labeled tomato lectin for imaging vasculature structures. *Histochem Cell Biol*. 2015;143:225–234. doi: 10.1007/s00418-014-1301-3
27. Teng B, Tilley SL, Ledent C, Mustafa SJ. In vivo assessment of coronary flow and cardiac function after bolus adenosine injection in adenosine receptor knockout mice. *Physiol Rep*. 2016;4:e12818. doi: 10.14814/phy2.12818
28. Semenza GL. Hypoxia-inducible factor 1 and cardiovascular disease. *Annu Rev Physiol*. 2014;76:39–56. doi: 10.1146/annurev-physiol-021113-170322
29. Schofield CJ, Ratcliffe PJ. Oxygen sensing by HIF hydroxylases. *Nat Rev Mol Cell Biol*. 2004;5:343–354. doi: 10.1038/nrm1366
30. Ivan M, Kondo K, Yang H, Kim W, Valiando J, Ohh M, Salic A, Asara JM, Lane WS, Kaelin WG. HIFalpha targeted for VHL-mediated destruction by proline hydroxylation: implications for O2 sensing. *Science*. 2001;292:464–468. doi: 10.1126/science.1059817
31. Ravi R, Mookerjee B, Bhujwalla ZM, Sutter CH, Artemov D, Zeng Q, Dillehay LE, Madan A, Semenza GL, Bedi A. Regulation of tumor angiogenesis by p53-induced degradation of hypoxia-inducible factor 1alpha. *Genes Dev*. 2000;14:34–44.
32. Nieminen AL, Qanungo S, Schneider EA, Jiang BH, Agani FH. Mdm2 and HIF-1alpha interaction in tumor cells during hypoxia. *J Cell Physiol*. 2005;204:364–369. doi: 10.1002/jcp.20406

33. Joshi S, Singh AR, Durden DL. MDM2 regulates hypoxic hypoxia-inducible factor 1α stability in an E3 ligase, proteasome, and PTEN-phosphatidylinositol 3-kinase-AKT-dependent manner. *J Biol Chem*. 2014;289:22785–22797. doi: 10.1074/jbc.M114.587493
34. Wu X, Bayle JH, Olson D, Levine AJ. The p53-mdm-2 autoregulatory feedback loop. *Genes Dev*. 1993;7:1126–1132. doi: 10.1101/gad.7.7a.1126
35. Linares LK, Hengstermann A, Ciechanover A, Müller S, Scheffner M. HdmX stimulates Hdm2-mediated ubiquitination and degradation of p53. *Proc Natl Acad Sci U S A*. 2003;100:12009–12014. doi: 10.1073/pnas.2030930100
36. Kubbutat MH, Jones SN, Vousden KH. Regulation of p53 stability by Mdm2. *Nature*. 1997;387:299–303. doi: 10.1038/387299a0
37. Geisterfer-Lowrance AA, Kass S, Tanigawa G, Vosberg HP, McKenna W, Seidman CE, Seidman JG. A molecular basis for familial hypertrophic cardiomyopathy: a beta cardiac myosin heavy chain gene missense mutation. *Cell*. 1990;62:999–1006. doi: 10.1016/0092-8674(90)90274-i
38. Geisterfer-Lowrance AA, Christe M, Conner DA, Ingwall JS, Schoen FJ, Seidman CE, Seidman JG. A mouse model of familial hypertrophic cardiomyopathy. *Science*. 1996;272:731–734. doi: 10.1126/science.272.5262.731
39. Camici PG, d'Amati G, Rimoldi O. Coronary microvascular dysfunction: mechanisms and functional assessment. *Nat Rev Cardiol*. 2015;12:48–62. doi: 10.1038/nrcardio.2014.160
40. Cecchi F, Olivotto I, Gistri R, Lorenzoni R, Chiriatti G, Camici PG. Coronary microvascular dysfunction and prognosis in hypertrophic cardiomyopathy. *N Engl J Med*. 2003;349:1027–1035. doi: 10.1056/NEJMoa025050
41. Olivotto I, Cecchi F, Gistri R, Lorenzoni R, Chiriatti G, Girolami F, Torricelli F, Camici PG. Relevance of coronary microvascular flow impairment to long-term remodeling and systolic dysfunction in hypertrophic cardiomyopathy. *J Am Coll Cardiol*. 2006;47:1043–1048. doi: 10.1016/j.jacc.2005.10.050
42. Olivotto I, Girolami F, Sciagrà R, Ackerman MJ, Sotgia B, Bos JM, Nistri S, Sgalambro A, Grifoni C, Torricelli F, et al. Microvascular function is selectively impaired in patients with hypertrophic cardiomyopathy and sarcomere myofilament gene mutations. *J Am Coll Cardiol*. 2011;58:839–848. doi: 10.1016/j.jacc.2011.05.018
43. Patterson DM, Gao D, Trahan DN, Johnson BA, Ludwig A, Barbieri E, Chen Z, Diaz-Miron J, Vassilev L, Shohet JM, et al. Effect of MDM2 and vascular endothelial growth factor inhibition on tumor angiogenesis and metastasis in neuroblastoma. *Angiogenesis*. 2011;14:255–266. doi: 10.1007/s10456-011-9210-8
44. Venkatesan T, Alaseem A, Chinnaiyan A, Dhandayuthapani S, Kanagasabai T, Alhazzani K, Dondapati P, Alobid S, Natarajan U, Schwartz R, et al. MDM2 overexpression modulates the angiogenesis-related gene expression profile of prostate cancer cells. *Cells*. 2018;7:41. doi: 10.3390/cells7050041
45. Hou H, Sun D, Zhang X. The role of MDM2 amplification and overexpression in therapeutic resistance of malignant tumors. *Cancer Cell Int*. 2019;19:216. doi: 10.1186/s12935-019-0937-4
46. Vignier N, Schlossarek S, Fraysse B, Mearini G, Kramer E, Pointu H, Mougenot N, Guiard J, Reimer R, Hohenberg H, et al. Nonsense-mediated mRNA decay and ubiquitin-proteasome system regulate cardiac myosin-binding protein C mutant levels in cardiomyopathic mice. *Circ Res*. 2009;105:239–248. doi: 10.1161/CIRCRESAHA.109.201251
47. Predmore JM, Wang P, Davis F, Bartolone S, Westfall MV, Dyke DB, Pagani F, Powell SR, Day SM. Ubiquitin proteasome dysfunction in human hypertrophic and dilated cardiomyopathies. *Circulation*. 2010;121:997–1004. doi: 10.1161/CIRCULATIONAHA.109.904557
48. Schlossarek S, Schuermann F, Geertz B, Mearini G, Eschenhagen T, Carrier L. Adrenergic stress reveals septal hypertrophy and proteasome impairment in heterozygous Mybpc3-targeted knock-in mice. *J Muscle Res Cell Motil*. 2012;33:5–15. doi: 10.1007/s10974-011-9273-6
49. Schlossarek S, Englmann DR, Sultan KR, Sauer M, Eschenhagen T, Carrier L. Defective proteolytic systems in Mybpc3-targeted mice with cardiac hypertrophy. *Basic Res Cardiol*. 2012;107:235. doi: 10.1007/s00395-011-0235-3
50. Wolf ER, Mabry AR, Damania B, Mayo LD. Mdm2-mediated neddylation of pVHL blocks the induction of antiangiogenic factors. *Oncogene*. 2020;39:5228–5239. doi: 10.1038/s41388-020-1359-4
51. Lv X, Li J, Zhang C, Hu T, Li S, He S, Yan H, Tan Y, Lei M, Wen M, et al. The role of hypoxia-inducible factors in tumor angiogenesis and cell metabolism. *Genes Dis*. 2017;4:19–24. doi: 10.1016/j.gendis.2016.11.003
52. Kimura W, Nakada Y, Sadek HA. Hypoxia-induced myocardial regeneration. *J Appl Physiol (1985)*. 2017;123:1676–1681. doi: 10.1152/japplphysiol.00328.2017
53. Menendez-Montes I, Escobar B, Palacios B, Gomez MJ, Izquierdo-Garcia JL, Flores L, Jimenez-Borreguero LJ, Aragones J, Ruiz-Cabello J, Torres M, et al. Myocardial VHL-HIF signaling controls an embryonic metabolic switch essential for cardiac maturation. *Dev Cell*. 2016;39:724–739. doi: 10.1016/j.devcel.2016.11.012
54. Camaioni C, Knott KD, Augusto JB, Seraphim A, Rosmini S, Ricci F, Boubertakh R, Xue H, Hughes R, Captur G, et al. Inline perfusion mapping provides insights into the disease mechanism in hypertrophic cardiomyopathy. *Heart*. 2020;106:824–829. doi: 10.1136/heartjnl-2019-315848
55. Hughes RK, Camaioni C, Augusto JB, Knott K, Quinn E, Captur G, Seraphim A, Joy G, Syrris P, Elliott PM, et al. Myocardial perfusion defects in hypertrophic cardiomyopathy mutation carriers. *J Am Heart Assoc*. 2021;10:e020227. doi: 10.1161/JAHA.120.020227
56. Tesic M, Beleslin B, Giga V, Jovanovic I, Marinkovic J, Trifunovic D, Petrovic O, Dobric M, Aleksandric S, Juricic S, et al. Prognostic value of transthoracic doppler echocardiography coronary flow velocity reserve in patients with asymmetric hypertrophic cardiomyopathy. *J Am Heart Assoc*. 2021;10:e021936. doi: 10.1161/JAHA.120.021936
57. Grier JD, Xiong S, Elizondo-Fraire AC, Parant JM, Lozano G. Tissue-specific differences of p53 inhibition by Mdm2 and Mdm4. *Mol Cell Biol*. 2006;26:192–198. doi: 10.1128/MCB.26.1.192-198.2006
58. Hauck L, Stanley-Hasnain S, Fung A, Grothe D, Rao V, Mak TW, Billia F. Cardiac-specific ablation of the E3 ubiquitin ligase Mdm2 leads to oxidative stress, broad mitochondrial deficiency and early death. *PLoS One*. 2017;12:e0189861. doi: 10.1371/journal.pone.0189861
59. Kouzu H, Tatekoshi Y, Chang HC, Shapiro JS, McGee WA, De Jesus A, Ben-Sahra I, Arany Z, Leor J, Chen C, et al. ZFP36L2 suppresses mTORc1 through a P53-dependent pathway to prevent peripartum cardiomyopathy in mice. *J Clin Invest*. 2022;132:e154491. doi: 10.1172/JCI154491
60. Ho CY, Day SM, Axelsson A, Russell MW, Zahka K, Lever HM, Pereira AC, Colan SD, Margossian R, Murphy AM, et al; VANISH Investigators. Valsartan in early-stage hypertrophic cardiomyopathy: a randomized phase 2 trial. *Nat Med*. 2021;27:1818–1824. doi: 10.1038/s41591-021-01505-4
61. Haeussler M, Schonig K, Eckert H, Eschstruth A, Mianne J, Renaud JB, Schneider-Maunoury S, Shkumatava A, Teboul L, Kent J, et al. Evaluation of off-target and on-target scoring algorithms and integration into the guide RNA selection tool CRISPOR. *Genome Biol*. 2016;17:148. doi: 10.1186/s13059-016-1012-2
62. Pelletier S, Gingras S, Green DR. Mouse genome engineering via CRISPR-Cas9 for study of immune function. *Immunity*. 2015;42:18–27. doi: 10.1016/j.immuni.2015.01.004
63. Nicolas N, Roux E. 3D Imaging and quantitative characterization of mouse capillary coronary network architecture. *Biology (Basel)*. 2021;10:306. doi: 10.3390/biology10040306
64. Robertson RT, Levine ST, Haynes SM, Gutierrez P, Baratta JL, Tan Z, Longmuir KJ. Use of labeled tomato lectin for imaging vasculature structures. *Histochem Cell Biol*. 2015;143:225–234. doi: 10.1007/s00418-014-1301-3
65. Chang WT, Fisch S, Chen M, Qiu Y, Cheng S, Liao R. Ultrasound based assessment of coronary artery flow and coronary flow reserve using the pressure overload model in mice. *J Vis Exp*. 2015;98:e52598. doi: 10.3791/52598
66. Teng B, Tilley SL, Ledent C, Mustafa SJ. In vivo assessment of coronary flow and cardiac function after bolus adenosine injection in adenosine receptor knockout mice. *Physiol Rep*. 2016;4:e12818. doi: 10.14814/phy2.12818
67. Soderberg O, Gullberg M, Jarvius M, Ridderstrale K, Leuchowius KJ, Jarvius J, Wester K, Hydbring P, Bahram F, Larsson LG, et al. Direct observation of individual endogenous protein complexes in situ by proximity ligation. *Nat Methods*. 2006;3:995–1000. doi: 10.1038/nmeth947